Analysing the effect of screw configuration using a stochastic twin-screw granulation model

Andrew D. McGuire[a], Sebastian Mosbach[a], Gavin K. Reynolds[b], Robert I. A. Patterson[c], Eric Bringley[a], Nick Eaves[a], Jochen A. H. Dreyer[a], Markus Kraft[a,d,*]

[a] *Department of Chemical Engineering and Biotechnology, University of Cambridge, Philippa Fawcett Dr, Cambridge, CB3 0AS, United Kingdom*
[b] *Pharmaceutical Technology & Development, AstraZeneca, Charter Way, Macclesfield, SK10 2NA, United Kingdom*
[c] *Weierstrass Institute for Applied Analysis and Stochastics, Mohrenstraße 39, Berlin 10117, Germany*
[d] *School of Chemical and Biomedical Engineering, Nanyang Technological University, 62 Nanyang Drive, Singapore 637459*

Abstract

In this work, a framework for modelling twin-screw granulation processes with variable screw configurations using a high-dimensional stochastic population balance method is presented. A modular compartmental approach is presented and a method for estimating residence times for model compartments based on screw element geometry is introduced. The model includes particle mechanisms for nucleation, primary particle layering, coalescence, breakage, and consolidation. A new twin-screw breakage model is introduced, which takes into account the differing breakage dynamics between two types of screw element. Additionally, a new sub-model for the layering of primary particles onto larger agglomerates is presented. The resulting model is used to simulate a twin-screw system with a number of different screw configurations and the predictive power of the model is assessed through comparison with an existing experimental data set in the literature. For most of the screw configurations simulated, the model predicts the product particle size distribution at large particle sizes with a reasonable degree of accuracy. However, the model has a tendency to over-predict

*Corresponding author
Email address: mk306@cam.ac.uk (Markus Kraft)

the amount of fines in the final product. Nevertheless, the model qualitatively captures the reduction in fines associated with an increase in the number of kneading elements, as observed experimentally. Based on model results, a number of key areas for future model development are identified and discussed.

Keywords: granulation, twin-screw, stochastic, population balance

1. Introduction

Twin-screw wet granulation (TSG) is a relatively new method of continuous granule manufacture. TSG devices, such as the one depicted in Figure 1, consist of two co-rotating screws enclosed within a barrel. The screws are constructed from an inter-changeable sequence of elements with various geometries. In the case of wet granulation, a solid blend of excipient/ active-pharmaceutical ingredient (API) and liquid binding agent are separately and continuously fed to the system. The solid and liquid phases interact in a high-shear environment of the screw barrel to create a potential mixture of granules and often some ungranulated powder mass, depending on the operating condition [1, 2, 3, 4]. The resulting granules find application as tabletting feed stock within the pharmaceutical industry, the fertiliser industry and foodstuffs [5].

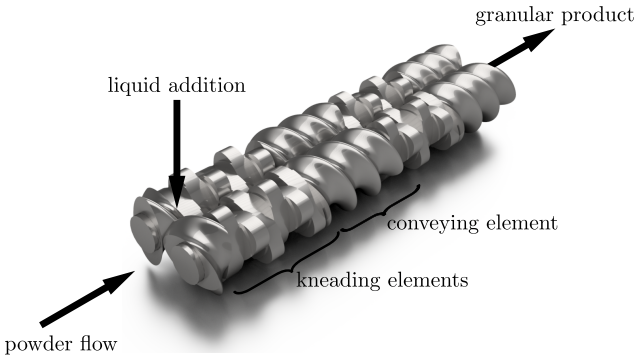

Figure 1: Variation zone of the a twin-screw granulator

TSG has a number of benefits over traditional batch granulation, namely, reduced plant footprint, ease of scale-up [6], the ability to create granules with

high drug loading [7] and a highly configurable set-up, primarily due to the variable screw configuration. However, the configurability of the device also creates a very large operating space for process optimisation during formulation, which can be problematic when only small quantities of API may be available. For this reason, a number of experimental studies [8, 3] have tried to investigate the relationship between the screw configuration, in terms of the number/position of certain types of element, and key properties of the product granules (such as particle size distribution (PSD), porosity and liquid distribution). Some studies have also focused on defining the role of specific types of screw element by using them in isolation [9, 2]. Experimental investigations into particle breakage in twin-screw devices [8, 10, 11, 3, 9] have highlighted the role of screw element geometry on the breakage dynamics along the barrel. For example, several studies [3, 9] have shown that the large agglomerates in conveying elements undergo size reduction through cutting or edge chipping, where small fragments are continually taken from the edge of the agglomerates. The particle size distribution transformation induced by distributive mixing elements (DME) in Pradhan et al. [9] suggests that breakage in these elements occurs through a combination of crushing and chipping [9].

Because of the combinatorial nature of the twin-screw operating space, it is desirable to develop a process model where the screw sections can be treated in a modular manner, such that the performance of new screw configurations may be quickly assessed without the usage of excipient/API or the need to set-up the device etc. This has generally been attempted through the use of compartmental population balance models (PBM) [12]. Several examples of compartmental twin-screw PBMs exist in the literature [13, 14, 15, 16, 17]. In these examples, the screw barrel domain is modelled as a number of connected compartments that permit process conditions and thus particle morphology to vary along the length of the simulation domain. These examples have used a sectional solution approach [18, 19, 20] which allows the compartmental PBM to be approximated and solved as a system of ordinary differential equations. This numerical approach generally limits the particle representation to taken

on three dimensions at most. The Stochastic particle method [21, 22, 23, 24, 25, 26, 27, 28] is alternative approach that has been employed to solve PBMs for batch granulation systems [29, 30, 31, 32, 33, 34, 35, 36, 37], silica [38] and TiO_2 [39] nano-particle synthesis, soot formation [40, 41], and more recently twin-screw granulation [42, 43]. Unlike sectional methods, stochastic particle methods permit much more complex particle representations, which can then be leveraged within the process model description, whilst still yielding a numerical problem that can be solved with acceptable levels of computational effort.

The main aims of this paper are:

1. Improve the stochastic TSG model in McGuire et al. [42, 43] based on the areas identified for improvement.

2. Construct a modelling framework that allows for the compartmental representation of arbitrary screw configurations and incorporates an element rate constant library. This library should contain optimised, re-usable, model rate parameters for different types of screw element.

3. Use the modelling framework to optimise a model parameter library against existing experimental data.

4. Assess the predictive ability of the complete model framework/parameter library using experimental data associated with a screw configuration not used in the optimisation of the library.

The remainder of the paper is structured as follows: firstly, the TSG PBM and a discussion of the compartmentalisation methodology are presented. The stochastic weighted particle method used to simulate the PBM is then presented in detail in Section 3. The experimental systems used for the optimisation step and the simulation conditions are described in Section 4. This is followed by a discussion of the model results in Section 5 and concluding remarks in Section 6.

2. Twin-screw population balance model

2.1. Particle type-space and population balance equation

In this TSG model, particles are described using the type-space $\mathbb{X}$. In $\mathbb{X}$, each element is characterised using a four-dimensional vector $x = (s_o, l_e, l_i, p) \in \mathbb{X}$ where: s_o is the volume of original solid, l_e is the volume of external liquid, l_i is the volume of internal liquid and p is the pore volume. The key derived particle properties are summarised in Table 1.

Table 1: Summary of derived particle properties. Here, ρ_s and ρ_l are the solid and liquid densities, respectively.

Property (Nomenclature)	Expression	Unit
Volume (v)	$s_o + l_e + p$	m^3
Diameter (d)	$(6v/\pi)^{1/3}$	m
Mass (m)	$\rho_s s_o + \rho_l(l_i + l_e)$	kg
Porosity (ε)	p/v	-
External surface area (a_{surf})	$\pi^{1/3}(6v)^{2/3}$	m^2

'Free' primary particles (i.e. those that are not part of an agglomerate) are comprised purely of original solid. Since the width of the primary particle size distribution is significantly smaller than that of the aggregate distribution of interest, these particles are modelled as a mono-disperse phase with representative particle diameter d_{pp} and volume v_{pp}. Furthermore, since the set of all primary particles $\mathbb{X}_{pp} \subset \mathbb{X}$ is only permitted to occupy a very limited region of the type-space ($\mathbb{X}_{pp} = \{x_{pp}\}, x_{pp} = (v_{pp}, 0, 0, 0)$) it is sufficient to characterise this phase by the number concentration of primary particles $c_{pp} \in \mathbb{R}^+$ or, equivalently, the number of primary particles $N_{pp} \in \mathbb{R}^+$ that exist within a given volume of the system to be modelled. The aggregate type space may then be defined as $\mathbb{X}_{agg} = \mathbb{X} \setminus \mathbb{X}_{pp}$.

Elements of $\mathbb{X}_{agg}$ take positions in a bounded domain of compartments. Similarly, each compartment has an associated number of primary particles N_{pp}. Each compartment is denoted by its index $z \in \mathbb{L}$. Particles (both primaries and

aggregates) are permitted to move between compartments according to the connections defined by the compartmentalisation of the system (discussed further in Section 2.4). Only particles within the same compartment are permitted to interact with each other.

This work uses the concept of deferred processes, as defined by the Linear Process Deferment Algorithm [44]. This algorithm is utilised to defer the applications of linear process operators that are particularly computationally intensive, such as the layering of primary particles onto the surface of large aggregates.

Since the population balance model is to be solved using the stochastic particle method, it is constructed in weak form. That is to say, each of the terms is integrated against some suitable test function. Let

1. $\lambda(z, t, \mathrm{d}x)$ be a concentration measure on $\mathbb{X}_{\mathrm{agg}}$ at time t in compartment z,

2. addition and subtraction on $\mathbb{X}$ correspond to particle coagulation and breakage, respectively,

3. $\varphi(z, x) : \mathbb{X} \mapsto \mathbb{R}$ be a suitable test function which is smooth with compact support,

4. $D_t : (\mathbb{L}, \mathbb{X}_{\mathrm{agg}}, \mathbb{R}^+) \mapsto \mathbb{X}_{\mathrm{agg}}$ be the aggregate deferment function that carries out the deferred aggregate processes. For any particle x, compartment z and primary particle concentration c_{pp}, $D_t(z, x, c_{\mathrm{pp}})$ is distributed as the value at time t of the Markov chain defined by the undeferred jump processes and their associated rates. In this way, $\mathbb{P}(D_t(z, x, c_{\mathrm{pp}}) = \mathrm{d}\xi)$ defines the probability that particle $D_t(z, x, c_{\mathrm{pp}})$ will lie within the type-space $[\xi, \xi + \mathrm{d}\xi]$.

The weak form of the aggregate PBE to be solved is then

$$\begin{aligned}\frac{\mathrm{d}}{\mathrm{d}t}\int_{x\in\mathbb{X}_{\mathrm{agg}}}\varphi(z,x)\lambda(z,t,\mathrm{d}x) &= \int_{x\in\mathbb{X}_{\mathrm{agg}}}\varphi(z,x)I_{\mathrm{nuc}}(z,t,c_{\mathrm{pp}},\mathrm{d}x) \\ &+\frac{1}{2}\int_{x,y,\xi,\zeta\in\mathbb{X}_{\mathrm{agg}}}[\varphi(z,\xi+\zeta)-\varphi(z,x)-\varphi(z,y)]K_{\mathrm{coag}}(z,\xi,\zeta) \\ &\qquad \mathbb{P}(D_t(z,x,c_{\mathrm{pp}})=\mathrm{d}\xi)\mathbb{P}(D_t(z,y,c_{\mathrm{pp}})=\mathrm{d}\zeta) \\ &\qquad \lambda(z,t,\mathrm{d}x)\lambda(z,t,\mathrm{d}y) \\ &+\frac{1}{2}\int_{x,y,\xi\in\mathbb{X}_{\mathrm{agg}}}[\varphi(z,\xi)+\varphi(z,\xi-y)-\varphi(z,x)]F(z,\xi,\mathrm{d}y) \\ &\qquad \mathbb{P}(D_t(z,x,c_{\mathrm{pp}})=\mathrm{d}\xi)\lambda(z,t,\mathrm{d}x) \\ &+\int_{x,\xi\in\mathbb{X}_{\mathrm{agg}}}\varphi(z,\xi)r_{\mathrm{inflow}}(z)\mathbb{P}(D_t(z-1,x,c_{\mathrm{pp}})=\mathrm{d}\xi)\lambda(z-1,t,\mathrm{d}x) \\ &-\int_{x,\xi\in\mathbb{X}_{\mathrm{agg}}}\varphi(z,\xi)\frac{1}{\tau(z)}\mathbb{P}(D_t(z,x,c_{\mathrm{pp}})=\mathrm{d}\xi)\lambda(z,t,\mathrm{d}x) \quad \forall z\in\mathbb{L},\end{aligned} \tag{1}$$

and corresponding primary particle PBE can be written as

$$\frac{\mathrm{d}}{\mathrm{d}t}c_{\mathrm{pp}}(z,t) = I_{\mathrm{trans,pp}}(z,t) - I_{\mathrm{nuc,pp}}(z,t) - \int_{x\in\mathbb{X}_{\mathrm{agg}}} r_{\mathrm{layer}}(z,t,x,c_{\mathrm{pp}})\lambda(z,t,\mathrm{d}x). \tag{2}$$

In this form, each integral on the RHS of Equation (1) represents an aggregate particle process within the model. In order of appearance in Equation (1), these are: nucleation, collision (which may lead to coagulation), breakage, inflow and outflow. The $\varphi(\cdot)$ component of each integrand represents the particle transformation associated with the related mechanism. The remainder of the integrand defines the rate at which this process occurs. In the primary particle PBE (Equation (2)) the terms, in order of their appearance on the RHS, represent inflow/outflow processes, nucleation and layering (onto aggregates). Each of the terms in Equation (1) and (2) will be fully defined for the TSG model in the section to follow. A visual interpretation of the particle processes introduced above is provided in Figure 2.

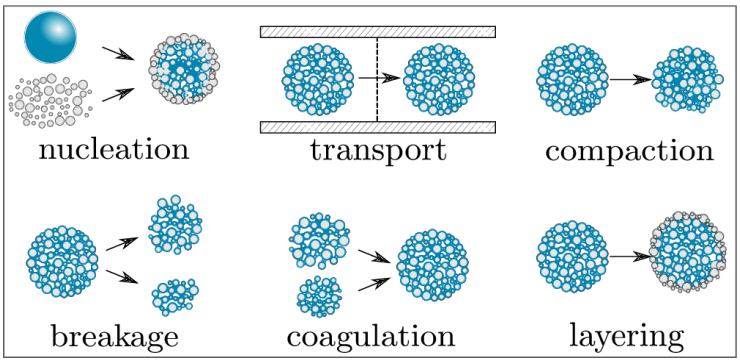

Figure 2: Twin-screw particle mechanisms. In this schematic, inflow and outflow processes have been combined into an overarching *transport* process.

2.2. Aggregate particle processes

The next section describes the form of the various kernels and operators in the aggregate PBE (1) in the context of the twin-screw model. Details of the implementation of these mechanisms including the jump transforms are presented later in Section 3.

2.2.1. Nucleation

The first term in Equation (1) represents the nucleation (formation) of aggregate particles. The nucleation process involves the addition of a liquid droplet to the first compartment and rapid addition of primary particles to the droplet, producing a nucleus particle with form $x_{\text{nuc}} \in \mathbb{X}_{\text{agg}}$.

As in [42], the nucleation model is formulated to resemble the process of a large liquid droplet (relative to the primary particle size) penetrating into a porous powder bed (immersion nucleation). Using this model, a nucleus incepted into compartment z takes the form

$$x_{\text{nuc}}(z, c_{\text{pp}}, t) = \begin{cases} \left(\dfrac{v_{\text{drop}}}{\phi_{\max}}, 0, v_{\text{drop}}, \dfrac{v_{\text{drop}}}{s^*} \right), & \text{if } \dfrac{v_{\text{drop}}}{\phi_{\max}} \leq c_{\text{pp}}(z) V_{\text{real}}(z) v_{\text{pp}}, \\ \left(c_{\text{pp}}(z) V_{\text{real}}(z) v_{\text{pp}},\ v_{\text{drop}} - c_{\text{pp}}(z) V_{\text{real}}(z) v_{\text{pp}} \phi_{\max}, \right. & \\ \quad \left. c_{\text{pp}}(z) V_{\text{real}}(z) v_{\text{pp}} \phi_{\max},\ \dfrac{c_{\text{pp}}(z) V_{\text{real}}(z) v_{\text{pp}} \phi_{\max}}{s^*} \right), & \text{otherwise.} \end{cases}$$

Here, $c_{\mathrm{pp}}(z)$ is the number concentration of primary particles in compartment z, s^* is the pore liquid saturation limit, $\phi_{\max}$ is maximum liquid saturation of solid material during nucleation and V_{real} is the physical volume of the compartment occupied by the granular mass (including the bed voidage), which sets the scale of the 'physical' system. v_{drop} is the number average volume of a droplet, which, in this study, takes the volume of a sphere with the same diameter as the liquid addition nozzle d_{nozzle}. As in McGuire et al. [42], the liquid saturation limit is given as

$$\phi_{\max} = \frac{(1-\varepsilon_{\mathrm{bed}})s^*}{\varepsilon_{\mathrm{bed}}}. \tag{3}$$

The two cases in (3) cover the situations in which:

i) there is sufficient primary particle mass in the droplet zone to permit formation of a complete nucleus particle

ii) there is insufficient primary particle mass in the droplet zone and a partially formed nucleus is created, which has a non-zero amount of external liquid

In the model, a single droplet creates a single nucleus particle, hence the nucleation rate $R_{\mathrm{nuc}}(z,t)$ is equal to the rate of droplet addition $R_{\mathrm{drop}}(z,t)$, which is defined as

$$R_{\mathrm{drop}}(z,t) = \begin{cases} \dfrac{(\mathrm{LSR})\dot{m}_{\mathrm{feed}}}{v_{\mathrm{drop}}\rho_{\mathrm{l}}}, & \text{if } z = 1, \\ 0, & \text{otherwise.} \end{cases} \tag{4}$$

Here, LSR is the operating liquid-solid mass feed ratio to the twin-screw device and $\dot{m}_{\mathrm{feed}}$ is the operating mass feed rate.

In the context of the aggregate PBE (1), one may define

$$I_{\mathrm{nuc}}(z,t,c_{\mathrm{pp}},\mathrm{d}x) = \frac{R_{\mathrm{nuc}}(z,t)\delta_{x_{\mathrm{nuc}}(z,c_{\mathrm{pp}},t)}(x)\mathrm{d}x}{V_{\mathrm{real}}(z)}, \tag{5}$$

where $\delta_{x_i}(x)$ is to be understood as the Dirac delta function, centred on x_i.

2.2.2. Collision and coagulation

The second term in the PBE (1) represents binary collisions and coagulation between particles. The collisions fall into the following categories:

1. Coagulating collision: collision pair forms a new aggregate particle

$$x_i, x_j \mapsto T_{\text{coag}}(x_i, x_j), \tag{6}$$

where, following the approach of Braumann et al. [30], the vector valued function $T_{\text{coag}}(x_i, x_j)$ is characterised as

$$T_{\text{coag}}(x_i, x_j) = (T_{\text{coag}}(x_i, x_j)_{s_\text{o}}, T_{\text{coag}}(x_i, x_j)_{l_\text{e}}, T_{\text{coag}}(x_i, x_j)_{l_\text{i}}, T_{\text{coag}}(x_i, x_j)_\text{p})^\top \tag{7}$$

with coordinate functions

$$T_{\text{coag}}(x_i, x_j)_{s_\text{o}} = s_\text{o}(x_i) + s_\text{o}(x_j) \tag{8}$$

$$T_{\text{coag}}(x_i, x_j)_{l_\text{e}} = l_\text{e}(x_i) + l_\text{e}(x_j) - l_{\text{e}\to\text{i}}(x_i, x_j) \tag{9}$$

$$T_{\text{coag}}(x_i, x_j)_{l_\text{i}} = l_\text{i}(x_i) + l_\text{i}(x_j) + l_{\text{e}\to\text{i}}(x_i, x_j) \tag{10}$$

$$\begin{aligned} T_{\text{coag}}(x_i, x_j)_p = & \frac{a^+_{\text{surf}}(x_i, x_j)^{\frac{3}{2}}}{6\pi^{1/2}} \\ & - \left[s_\text{o}(x_i) + s_\text{o}(x_j) - l_\text{e}(x_i) - l_\text{e}(x_j) + l_{\text{e}\to\text{i}}(x_i, x_j)\right]. \end{aligned} \tag{11}$$

Here $l_{\text{e}\to\text{i}}(x_i, x_j)$ represent the amount of surface liquid that is internalised due to the contact area between the colliding particle pair. This is computed as [30]

$$\begin{aligned} l_{\text{e}\to\text{i}}(x_i, x_j) = \Bigg\{ & l_\text{e}(x_i) l_\text{e}(x_j) \left[1 - \sqrt{1 - \left(\frac{\sqrt[3]{v(x_i)} - l_\text{e}(x_i)}{\sqrt[3]{v(x_i)} + \sqrt[3]{v(x_j)}}\right)^2}\right] \\ & \times \left[1 - \sqrt{1 - \left(\frac{\sqrt[3]{v(x_j)} - l_\text{e}(x_j)}{\sqrt[3]{v(x_i)} + \sqrt[3]{v(x_j)}}\right)^2}\right] \Bigg\}^{1/2}, \end{aligned} \tag{12}$$

and

$$\begin{aligned} a^+_{\text{surf}}(x_i, x_j) = & (1 - e_\text{coag}) \left[a_\text{surf}(x_i)^{3/2} + a_\text{surf}(x_j)^{3/2}\right]^{2/3} \\ & + e_\text{coag} \left[a_\text{surf}(x_i) + a_\text{surf}(x_j)\right], \end{aligned} \tag{13}$$

and e_coag is the coefficient of restitution of the granular material.

2. Non-coagulating collision: colliding pairs do not coalescence and the collision pair remain unchanged

$$x_i, x_j \mapsto x_i, x_j. \tag{14}$$

Upon collision of two aggregates, the collision is deemed to be successful (i.e. coagulation takes place) provided that the colliding particles meet the Stokes criterion as detailed in Braumann et al. [30], otherwise the collision is non-coagulating and the colliding particles remain unchanged. The Stokes criterion takes into account the material coefficient of restitution e_{coag} and the amount of surface liquid present, relative to the presumed height of asperities on the surface of the aggregates h_{a}.

Particles collide according to the size-dependent collision kernel K_{col}, which takes the form

$$K_{\text{col}}(z, x_i, x_j) = k_{\text{col}}(z) n_{\text{screw}} C(d(x_i), d(x_j)) \tag{15}$$

$$\tag{16}$$

Here, $k_{\text{col}}(z)$ is the collision rate constant in compartment z, n_{screw} is the screw speed, and $C(d_1, d_2)$ is the collision rate function which defines the collision frequency between particles with diameter d_1 and d_2, respectively.

In this work, the Equi-partition of kinetic energy collision rate function [45] is used, which takes the form

$$C(d_i, d_j) = (d_i + d_j)^2 \sqrt{\frac{1}{d_i^3} + \frac{1}{d_j^3}}. \tag{17}$$

Studies using the Discrete Element Method (DEM) [46] have shown that the form of the collision function in (17) adequately describes the collision dynamics within batch granulation systems [47]. Furthermore, preliminary twin-screw simulations with this form of collision rate function showed that it promoted collisions between large agglomerates and primary particles over those between

particles which were similar in size. Thus, in the absence of an existing twin-screw specific collision kernel, the kernel in Equation (17) was deemed acceptable for the purposes of aggregate collisions and layering (to be introduced in Section 2.2.5).

The coagulation kernel K_{coag} of PBE (1) is then

$$K_{\text{coag}}(z, x_i, x_j) = K_{\text{col}}(z, x_i, x_j)\mathbb{1}_{\{x_i, x_j | \text{St}_\text{v}(x_i, x_j) \leq \text{St}^*_\text{v}(x_i, x_j)\}}(x_i, x_j), \tag{18}$$

where $\text{St}_\text{v}(x_i, x_j) \leq \text{St}^*_\text{v}(x_i, x_j)$ indicates that the Stokes criterion has been met and $\mathbb{1}_{\mathbb{A}}$ is to be understood as the indicator function of set $\mathbb{A}$,

2.2.3. Breakage

The third term in PBE (1) represents the aggregate breakage process. In this work, aggregates may undergo binary breakage according to the transform

$$x \mapsto x - y, y \tag{19}$$

at rate

$$g_{\text{break}}(z, x) = \begin{cases} k_{\text{att}}(z) n^2_{\text{screw}} \left(\dfrac{v(x)}{\hat{v}_{\text{break}}} \right)^{\omega_{\text{att}}(z)}, & \text{if } v(x) \geq v^{\text{min}}_{\text{parent}} \text{ and } l_\text{e}(x) + l_\text{i}(x) + p(x) \neq 0, \\ 0 & \text{otherwise,} \end{cases} \tag{20}$$

where k_{att} is the attrition rate constant, $v^{\text{min}}_{\text{parent}}$ is the minimum agglomerate size that can undergo breakage, ω_{att} is the breakage rate exponent and $\hat{v}_{\text{break}}$ is a normalisation parameter. In this work, $v^{\text{min}}_{\text{parent}} = v_{\text{pp}}$. The breakage of primary particles is not permitted in the current model.

In the context of the aggregate PBE (1), the breakage kernel takes the form [37]

$$F(z, x, \mathrm{d}y) = \mathbb{1}_{\{x, y | m(y) < m(x)\}}(x) g_{\text{break}}(z, x) B_{\text{frag}}(z, x, \mathrm{d}y), \tag{21}$$

where $B_{\text{frag}}(z, x, \mathrm{d}y)$ is the probability that the first particle formed from the breakage of particle x (according to (20)) lies within the space $[y, y + \mathrm{d}y]$. $B_{\text{frag}}(z, x, \mathrm{d}y)$ is characterised by first considering the probability distribution

of the volume of daughter particle y (denoted v_y). In this work, this is defined as

$$v_y(z, x, \chi_{\text{frag}}) = v^{\min}_{\text{parent}} + \chi_{\text{frag}} \left[v(x) - v^{\min}_{\text{parent}} \right], \tag{22}$$

where, following Braumann et al. [30], χ_{frag} is a random measure with beta distribution $f(z, \chi_{\text{frag}})$ with skewness parameters $\alpha_{\text{daughter}}(z)$ and $\beta_{\text{daughter}}(z)$.

As in previous granulation works [30, 36], it is assumed that the composition of the abraded particles y and $x - y$ are the same as x. Hence, y can be defined as

$$\mathrm{d}y = \frac{v_y(z, x, \mathrm{d}\chi_{\text{frag}})}{v(x)} x. \tag{23}$$

As mentioned in Section 1, conveying elements have been observed to break particles through cutting and edge chipping. No daughter distribution breakage data is currently available for kneading elements. However, based on their somewhat similar geometry, it is expected that the primary breakage mechanism in these elements will be similar to that in so called distributive mixing elements (DME) [2]. In this work, it is hypothesised that the primary breakage mechanisms in kneading elements will be the crushing behaviour observed in DME, with less emphasis on the chipping mechanism, due to the absence of the pronounced blades that are present in DME. To incorporate this information into the model, breakage exponent and daughter distribution parameters differ between different types of compartment (or, equivalently, screw element). The probability density distribution for χ_{frag} used for each element in this study are illustrated in Figure 3.

2.2.4. Aggregate transport

The fourth and fifth terms in the PBE (1) represent aggregate inflow and outflow processes on compartment z, respectively. Agglomerates and primary particles are permitted to flow uni-directionally along the network of compartments from the feed zone to the exit zone. Each compartment is modelled as a perfectly stirred tank such that each particle flows out of compartment z with

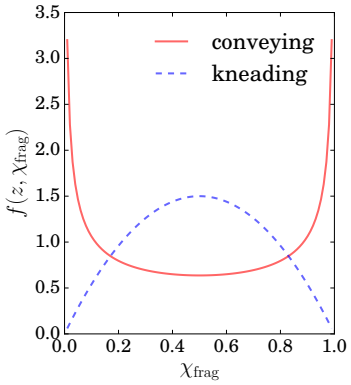

Figure 3: Element specific probability density functions for agglomerate breakage. In compartments that represent pure conveying zones $\alpha_{\text{daughter}} = \beta_{\text{daughter}} = 0.5$ and those representing pure kneading zones $\alpha_{\text{daughter}} = \beta_{\text{daughter}} = 2$.

rate $1/\tau(z)$, where $\tau(z)$ is the compartment residence time. Similarly, aggregate particles flow into compartment z from compartment $z-1$ at rate r_{inflow} where

$$r_{\text{inflow}}(z) = \begin{cases} 1/\tau(z-1) & \text{if } z > 1 \\ 0 & \text{otherwise.} \end{cases} \tag{24}$$

2.2.5. Continuous, deferred aggregate processes

A number of particle mechanisms are modelled as continuous processes that act on the agglomerates (and indirectly on the primary particles) in the system according to the deferment function $D_t : (\mathbb{L}, \mathbb{X}_{\text{agg}}, \mathbb{R}^+) \mapsto \mathbb{X}_{\text{agg}}$ introduced in Section 2.1.

These processes are:

1. Layering

   Layering is the process by which primary particles attach to the surface of the agglomerates. This process is modelled as a collision between agglomerates and primary particles using the same size-dependent collision kernel used for aggregate coagulation (Equation (15)).

   Layering is only permitted on agglomerates which have a volume of ex-

ternal liquid with height h_l exceeding the fixed height of asperities of the agglomerate particles h_a. The height of the external liquid on particle x is defined as

$$h_\mathrm{l}(x) = \frac{1}{2}\sqrt[3]{\frac{6}{\pi}}\left[\sqrt[3]{v(x)} - \sqrt[3]{v(x) - l_\mathrm{e}(x)}\right]. \tag{25}$$

In the current model, a successful layering event is supposed to 'dry out' the surface of the agglomerate particle. This drying is captured by the transformation of external liquid to internal liquid. For the addition of a single primary particle onto the surface of an agglomerate, the amount of liquid moved from the exterior to the interior is modelled as

$$l_{\mathrm{e}\to\mathrm{i}}(x) = \min(v_\mathrm{pp}, \pi d_\mathrm{pp}^2 h_\mathrm{l}(x)). \tag{26}$$

The form of (26) was constructed to cover the situations where the agglomerate surface is liquid rich and liquid poor. In the liquid rich case, a small primary may become fully immersed in the thick binder layer. In liquid poor situation, the primary particle is more likely to simply stick to the surface, hence the amount of internalisation is hypothesised to be proportional to the projected area of the primary.

It follows from the definitions above that the agglomerate particle x undergoes layering with rate

$$r_\mathrm{layer}(z, t, c_\mathrm{pp}, x) = \begin{cases} c_\mathrm{pp}(z,t) K_\mathrm{col}(z, d(x), d_\mathrm{pp}), & \text{if } \; h_\mathrm{l}(x) > h_\mathrm{a}, \\ 0, & \text{otherwise}, \end{cases} \tag{27}$$

and the rates of change of each particle property induced by the layering process are

$$\left.\frac{\mathrm{d}s_\mathrm{o}(x)}{\mathrm{d}t}\right|_\mathrm{layer} = r_\mathrm{layer}(z, x, c_\mathrm{pp}, t) v_\mathrm{pp}, \tag{28}$$

$$\left.\frac{\mathrm{d}l_\mathrm{e}(x)}{\mathrm{d}t}\right|_\mathrm{layer} = -r_\mathrm{layer}(z, x, c_\mathrm{pp}, t) l_{\mathrm{e}\to\mathrm{i}}(x), \tag{29}$$

$$\left.\frac{\mathrm{d}l_\mathrm{i}(x)}{\mathrm{d}t}\right|_\mathrm{layer} = r_\mathrm{layer}(z, x, c_\mathrm{pp}, t) l_{\mathrm{e}\to\mathrm{i}}(x), \tag{30}$$

$$\left.\frac{\mathrm{d}p(x)}{\mathrm{d}t}\right|_\mathrm{layer} = r_\mathrm{layer}(z, x, c_\mathrm{pp}, t) l_{\mathrm{e}\to\mathrm{i}}(x). \tag{31}$$

2. Consolidation

Consolidation of particles within the twin-screw system is presumed to occur primarily due to impacts between the particles and screw and walls of the barrel. The consolidation process is modelled as the reduction in particle porosity and subsequent squeezing of the internal liquid to the surface. It is presumed that the rate of consolidation is dependent on the screw speed and the geometry of the screw element in which the process is taking place. Since the effect of screw speed is not being investigated in this study, a simple consolidation model is employed. This takes the form:

$$\left.\frac{\mathrm{d}\varepsilon(x)}{\mathrm{d}t}\right|_{\text{consol}} = -k_{\text{comp}}(z) n_{\text{screw}} [\varepsilon(x) - \varepsilon_{\min}], \tag{32}$$

where $k_{\text{comp}}(z)$ is the compaction rate constant in compartment z and $\varepsilon_{\min}$ is the minimum porosity permitted for agglomerate particles.

The associated changes in the tracked particle properties due to consolidation are

$$\left.\frac{\mathrm{d}s_{\text{o}}(x)}{\mathrm{d}t}\right|_{\text{consol}} = 0, \tag{33}$$

$$\left.\frac{\mathrm{d}l_{\text{e}}(x)}{\mathrm{d}t}\right|_{\text{consol}} = -\frac{l_{\text{i}}(x)}{p(x)} \frac{\mathrm{d}p(x)}{\mathrm{d}t}, \tag{34}$$

$$\left.\frac{\mathrm{d}l_{\text{i}}(x)}{\mathrm{d}t}\right|_{\text{consol}} = -\frac{\mathrm{d}l_{\text{e}}(x)}{\mathrm{d}t}, \tag{35}$$

$$\left.\frac{\mathrm{d}p(x)}{\mathrm{d}t}\right|_{\text{consol}} = v(x) \frac{\mathrm{d}\varepsilon(x)}{\mathrm{d}t}. \tag{36}$$

Note that this has no effect on the primary particles since they have an $\varepsilon = 0$.

The aggregate deferment function D_t maps a particle x and primary particle concentration measure $c_{\text{pp}}(z)$ in z at time t_p to a particle $D_t(z, x, c_{\text{pp}})$ with time t (where t_p is the current time of particle x, $t_p \leq t$). This is done by evolving x

in time according to the rates

$$\left.\frac{\mathrm{d}s_{\mathrm{o}}(x)}{\mathrm{d}t}\right|_{\mathrm{defer}} = \left.\frac{\mathrm{d}s_{\mathrm{o}}(x)}{\mathrm{d}t}\right|_{\mathrm{layer}} + \left.\frac{\mathrm{d}s_{\mathrm{o}}(x)}{\mathrm{d}t}\right|_{\mathrm{consol}}, \tag{37}$$

$$\left.\frac{\mathrm{d}l_{\mathrm{e}}(x)}{\mathrm{d}t}\right|_{\mathrm{defer}} = \left.\frac{\mathrm{d}l_{\mathrm{e}}(x)}{\mathrm{d}t}\right|_{\mathrm{layer}} + \left.\frac{\mathrm{d}l_{\mathrm{e}}(x)}{\mathrm{d}t}\right|_{\mathrm{consol}}, \tag{38}$$

$$\left.\frac{\mathrm{d}l_{\mathrm{i}}(x)}{\mathrm{d}t}\right|_{\mathrm{defer}} = \left.\frac{\mathrm{d}l_{\mathrm{i}}(x)}{\mathrm{d}t}\right|_{\mathrm{layer}} + \left.\frac{\mathrm{d}l_{\mathrm{i}}(x)}{\mathrm{d}t}\right|_{\mathrm{consol}}, \tag{39}$$

$$\left.\frac{\mathrm{d}p(x)}{\mathrm{d}t}\right|_{\mathrm{defer}} = \left.\frac{\mathrm{d}p(x)}{\mathrm{d}t}\right|_{\mathrm{layer}} + \left.\frac{\mathrm{d}p(x)}{\mathrm{d}t}\right|_{\mathrm{consol}}. \tag{40}$$

Hence, if

$$\left.\frac{\mathrm{d}x}{\mathrm{d}t}\right|_{\mathrm{defer}} = \left(\left.\frac{\mathrm{d}s_{\mathrm{o}}(x)}{\mathrm{d}t}\right|_{\mathrm{defer}}, \left.\frac{\mathrm{d}l_{\mathrm{e}}(x)}{\mathrm{d}t}\right|_{\mathrm{defer}}, \left.\frac{\mathrm{d}l_{\mathrm{i}}(x)}{\mathrm{d}t}\right|_{\mathrm{defer}}, \left.\frac{\mathrm{d}p(x)}{\mathrm{d}t}\right|_{\mathrm{defer}} \right)^{\top}, \tag{41}$$

then

$$D_t(z, x, c_{\mathrm{pp}}) = x + \int_{t_p}^{t} \left.\frac{\mathrm{d}x}{\mathrm{d}t}\right|_{\mathrm{defer}} \mathrm{d}t. \tag{42}$$

215 *2.3. Primary particle processes*

This section describes each of the operators in the primary particle PBE (Equation (2)).

The first term in Equation (2) represents the transport operator (inflow and outflow) acting on the primary particles phase in compartment z. This is characterised by

$$I_{\mathrm{trans,pp}}(z,t) = \begin{cases} \left[\dfrac{\dot{m}_{\mathrm{feed}}}{v_{\mathrm{pp}}\rho_{\mathrm{s}}} - \dfrac{N_{\mathrm{pp}}(z)}{\tau(z)}\right] \dfrac{1}{V_{\mathrm{real}}(z)}, & \text{if } z = 1, \\ \left[\dfrac{N_{\mathrm{pp}}(z-1)}{\tau(z-1)} - \dfrac{N_{\mathrm{pp}}(z)}{\tau(z)}\right] \dfrac{1}{V_{\mathrm{real}}(z)} & \text{otherwise.} \end{cases} \tag{43}$$

The second term in Equation (2) represents the nucleation sink term, which complements the aggregate nucleation model by taking the form

$$I_{\mathrm{nuc,pp}}(t,z) = \begin{cases} \dfrac{\dot{m}_{\mathrm{feed}}\mathrm{LSR}}{v_{\mathrm{pp}}\rho_{\mathrm{l}}\phi_{\max}V_{\mathrm{real}}(z)}, & \text{if } z = 1, \\ 0, & \text{otherwise.} \end{cases} \tag{44}$$

The final term in (2) accounts for the depletion of primary particles through the deferred aggregate layering process (Equations (27)-(31)).

2.4. Compartmentalisation

In this paper, each compartment represents exactly one type of screw element. However, a screw element may be represented by more or less than one compartment (as demonstrated in Figure 4). As such, the total number of compartments employed may vary depending on the screw configuration being modelled. This allows increased resolution in areas where the changes in particle characteristics along the screw length are expected to be significant, such as the region around the liquid inception port. This is also the case in regions where the material flow is expected to more closely resemble a plug-flow, with limited back mixing, such as kneading elements.

As in existing twin-screw modelling efforts, it is assumed that the material undergoes very little change prior to the point of liquid inception (termed the "metering" zone), hence the screw configuration is modelled from the liquid inlet port on-ward (termed the "variation" zone). This liquid inception zone (droplet zone) in modelled as a conveying compartment with length 0.33D (where D is the diameter of the screw) which serves as the first compartment in all screw configurations investigated. An example of the compartmentalisation of a screw configuration used in this study is presented in Figure 4.

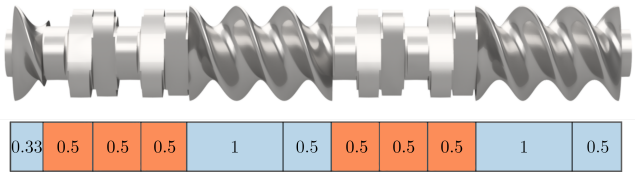

Figure 4: Example screw configuration (variation zone only) and the associated compartmental representation. The number in the centre of each compartment represents the compartment length (normalised by the screw diameter). Compartments representing conveying zones are in blue and compartments representing kneading zones are shown in orange.

2.5. Residence time estimation

The compartment residence times $\tau(z)$ that control the aggregate and primary particle flow rates are dependent on the compartmentalisation of the screw

and the operating conditions. In previous TSG modelling studies, compartmental residence times have been estimated through the use of DEM [48] and chemical imaging techniques [49, 50, 15]. In the case where DEM has been used, the PBM and DEM solvers are coupled, allowing collision statistics [51] and residence time estimation to be made, however, the significant computational cost of the DEM step negatively impacts the overall time required to solve the model. Hence, it is advantageous to have the ability to estimate the residence time of individual compartments simply from the screw configuration and device operation (mass and liquid flow rates). It is worth noting that, in studies of alternative granulation devices, such as Barrasso et al. [52], the costly DEM step has been replaced by an Artificial Neural Net (ANN) with promising results, though a sizeable amount of DEM data must be gathered to train such networks.

In order to create a framework for the prediction of residence times, information from a number of existing twin-screw material flow studies must be considered. A number of experimental studies have examined the mass distribution over the twin-screw system, through the use of Positron Emission Particle Tracking (PEPT) [53, 54]. Recently, it has also been proposed [55] that barrel fill level be used as way to define the design space in TSG. This has been motivated by the observation that very similar PSDs can be obtained for very different screw speed and mass feed rates, provided the fill level is the same across these experiments. From a screw element perspective, it is noted that, as a result of their geometry, it is noted that kneading elements will generally be completely or almost completely filled with material at steady state. This is because the kneading element geometry affords low conveying capacity, which allows for the accumulation of material. In contrast, conveying elements generally have a much lower fill level that is dependent on the operating speed of the screw [53] and the feed material [56]. This non-uniformity in the mass distribution ultimately leads to varying residence times across different sections of the screw, which must be captured within a model, if model rates are to be applied to various screw configurations. Attempts have been made to predict such mass

distribution in the context of twin-screw extrusion systems [57]. Though the resulting models showed good performance, the flowing material consisted of a polymer melt, which has quite different flow characteristics compared to the partially wet powder mass in the TSG system. This limits its applicability to TSG.

In order to be able to produce reasonable estimates of particle residence times of screw sections and model compartments for arbitrary screw configurations, a novel but simplistic approach was developed for use in this study. The approach involves two key stages: firstly the mean residence time of the complete device τ_{screw} is linearly interpolated from existing experimental data based on the screw configuration, screw speed and mass feed rate. In the second stage, this total device residence time is distributed over the compartmental network by estimating the mass distribution profile across the compartments. This work uses data from the residence time analysis experiments performed by Kumar et al. [49]. In that study, the authors used a chemical imaging approach where a dye-impulse was introduced into the powder feed zone in order to extract residence time distributions. These residence time estimates consider the full screw (i.e. both metering and variation zones) and the metering zone consisted purely of conveying elements.

The total mean screw residence time is split into the contribution from the metering zone and the variation zone as

$$\tau_{\text{screw}} \approx \tau_{\text{metering}} + \tau_{\text{variation}}. \tag{45}$$

Assuming that each section behaves as perfect plug-flow with no back-mixing then,

$$\tau_{\text{screw}} \approx \frac{M_{\text{metering}}}{\dot{m}_{\text{feed}}} + \frac{M_{\text{variation}}}{\dot{m}_{\text{feed}}(1 + \text{LSR})}, \tag{46}$$

where M_{metering} and $M_{\text{variation}}$ are dynamic mass hold-up (i.e. the mass of material that is not 'stuck' to the barrel wall and screws) within the metering

and variation zones, respectively. These are given as

$$M_{\text{metering}} = \sum_{i=1}^{N_{\text{m,convey}}} L_{\text{m,convey}}(i)\nu_{\text{convey}}\varepsilon_{\text{bed}}\rho_{\text{s}}f_{\text{m,convey}}(i), \tag{47}$$

$$M_{\text{variation}} = \sum_{i=1}^{N_{\text{v,convey}}} L_{\text{v,convey}}(i)\nu_{\text{convey}}\varepsilon_{\text{bed}}\rho_{\text{eff}}f_{\text{v,convey}}(i) + \sum_{i=1}^{N_{\text{v,knead}}} L_{\text{v,knead}}(i)\nu_{\text{knead}}\varepsilon_{\text{bed}}\rho_{\text{eff}}f_{\text{v,knead}}(i) \tag{48}$$

where the subscripts m and v refer to the metering and variation zones respectively and

- $N_{\text{j,convey}}$ is the number of conveying elements in zone j;
- $N_{\text{j,knead}}$ is the number of kneading elements in zone j;
- $L_{\text{j,e}}(i)$ is the length of the i^{th} screw section consisting of element type e in zone j (measured in screw diameters D);
- ν_{e} is the specific volume available in a screw section with element type e (measured in unit volume/length in screw diameters D);
- $f_{\text{j,e}}(i)$ is the volumetric fill fraction of the i^{th} screw section consisting of element type e in zone j;
- ρ_{eff} is the effective density of the solid material being held up in the variation zone;

For simplicity, it is assumed that ρ_{eff} is constant along the length of the variation zone. The effective density is computed as the weighted averaged density of the solid and liquid feed such that:

$$\rho_{\text{eff}} = \frac{(\text{LSR}+1)\rho_s\rho_l}{\rho_l + \rho_s\text{LSR}}. \tag{49}$$

Again, ρ_s is the density of solid feed material and ρ_l is the density of the liquid binder.

It is imposed that all kneading elements are filled to capacity with material (i.e. $f_{\mathrm{v,knead}}(i) = f_{\mathrm{v,knead}} = 1 \; \forall \; i \in \{1, \ldots, N_{\mathrm{v,knead}}\}$). Though PEPT studies [53] have shown that conveying elements that precedes a kneading element will generally have a higher fill fraction, for the purposes of the residence time estimation in this paper it is assumed that each compartment of element type e has the same fill fraction, such that $f_{\mathrm{m,convey}}(i) = f_{\mathrm{v,convey}}(k) = f_{\mathrm{convey}} \; \forall \; i \in \{1, \ldots, N_{\mathrm{m,convey}}\}, k \in \{1, \ldots, N_{\mathrm{v,convey}}\}$. This assumption permits f_{convey} to be solved by substitution of (47) and (48) into (46) and re-arranging to yield

$$f_{\mathrm{convey}} = \frac{\tau_{\mathrm{screw}} \dot{m}_{\mathrm{feed}}(1 + \mathrm{LSR}) - f_{\mathrm{v,knead}} \varepsilon_{\mathrm{bed}} \nu_{\mathrm{knead}} \sum_{i=1}^{N_{\mathrm{v,knead}}} L_{\mathrm{v,knead}}(i)}{\varepsilon_{\mathrm{bed}} \nu_{\mathrm{convey}} \left[\rho_s (1 + \mathrm{LSR}) \sum_{i=1}^{N_{\mathrm{m,convey}}} L_{\mathrm{m,convey}}(i) + \rho_{\mathrm{eff}} \sum_{i=1}^{N_{\mathrm{v,convey}}} L_{\mathrm{v,convey}}(i) \right]}. \tag{50}$$

Assuming that kneading elements are filled to capacity, knowledge of f_{convey} specifies the mass distribution across the full screw.

Given that compartment z represents a section of the screw composed of elements of type e, with length $L(z)$ and steady state mass hold-up $M(z)$ then the compartment residence time is approximated as

$$\tau(z) := \frac{M(z)}{\dot{m}_{\mathrm{feed}}} \tag{51}$$

$$= \frac{L(z) \nu_{\mathrm{e}} \varepsilon_{\mathrm{bed}} \rho_{\mathrm{eff}} f_{\mathrm{v,e}}}{\dot{m}_{\mathrm{feed}}}. \tag{52}$$

Since no residence time data was presented for pure conveying screws in Kumar et al. [49], residence times for such screw configurations was estimated using the derived steady state fill fraction predicted using the above flow model applied to a configuration with two kneading blocks (13.3%).

Derived fill fractions for conveying elements ranged from 10 - 13.3%, and overall derived fill levels between 13.3 - 24.1% with $\epsilon_{\mathrm{bed}} = 0.3$, depending on the screw configuration. This gives the fraction of screw bed occupied by material (i.e. discounting the packing fraction) as 4-7.23%. These values are lower than the ranges observed in alternative twin-screw devices (10-30%) [58], however, the method presented in this paper does not account for non-dynamic mass (i.e. material that is stuck to the walls), which could be significant as demonstrated

in other experimental studies [56].

Given a fill fraction for each element type, the real volume of material (including the bed voidage) modelled in each compartment $V_{\text{real}}(z)$ is computed as

$$V_{\text{real}}(z) = L(z)\nu_{\text{e}} f_{\text{v,e}}. \tag{53}$$

3. Numerical treatment

3.1. Stochastic particle methods for twin-screw granulation

The aggregate phase of the twin-screw population balance model is solved using the stochastic weighted algorithm (SWA) [21, 59, 24, 23]. The SWA has been successfully employed to solve population balance problems in the fields of granulation [47], soot formation, aerosol and nano-particle synthesis [38, 60, 39] and more general coagulation/fragmentation processes [25]. In the SWA, each compartment z is simulated with a discrete list of computational particles

$$(z, x_i, w_i), \quad i = 1, \ldots, N_{\text{agg}}(z,t), \tag{54}$$

which describes the population dynamics in (1). In (54), $x \in \mathbb{X}_{\text{agg}}$, $w_i \in (0, w_{\max}]$ is the statistical weight of the particle with index i and $N_{\text{agg}}(z,t)$ is the total number of aggregate stochastic particles in compartment z at time t. w can be thought of as indicator of the number of physical particles that are represented by computational particle (z, x, w). Each simulated compartment has an associated scaling parameter or sample volume denoted $V_{\text{sample}}(z,t)$ and the measure valued solution λ to the population balance equation (1) is approximated by the stochastic particle systems such that, for all φ ins a large class of test functions

$$\frac{1}{V_{\text{samp}}(z,t)} \sum_{i=1}^{N_{\text{agg}}(z,t)} w_i \varphi(z, x_i) \xrightarrow[V_{\text{samp}}(z,0)\to\infty]{} \int_{\mathbb{X}_{\text{agg}}} \varphi(z,x)\lambda(t,z,\mathrm{d}x) \tag{55}$$

and the initial sample volume (i.e. that at $t = 0$) is characterised by

$$\frac{1}{V_{\text{samp}}(z,0)} \sum_{i=1}^{N_{\text{agg}}(z,0)} w_i \approx \int_{\mathbb{X}_{\text{agg}}} \lambda(t,z,\mathrm{d}x). \tag{56}$$

The system of stochastic particles is evolved in time through a Markov jump process. This process is characterised by the possible jumps and their associated rates. Each available jump and the associated rate is a function of the state of the system at that point in time. At each t there exists a list of possible jumps which have independent, exponentially distributed waiting times. The waiting time between any two jumps Δt_{wait} is described by the distribution [61]:

$$\mathbb{P}(t, \Delta t_{\text{wait}} \geq \theta) = \exp\big(-R^{\text{SWA}}_{\text{total}}(t)\theta\big), \quad \theta \geq 0, \tag{57}$$

where $R^{\text{SWA}}_{\text{total}}$ is the total jump rate, which has the form

$$R^{\text{SWA}}_{\text{total}}(z,t) = R^{\text{SWA}}_{\text{nuc}}(z,t) + R^{\text{SWA}}_{\text{break}}(z,t) + R^{\text{SWA}}_{\text{trans}}(z,t) + R^{\text{SWA}}_{\text{coag}}(z,t). \tag{58}$$

Here, $R^{\text{SWA}}_{\text{nuc}}(z,t)$, $R^{\text{SWA}}_{\text{break}}(z,t)$, $R^{\text{SWA}}_{\text{trans}}(z,t)$ and $R^{\text{SWA}}_{\text{coag}}(z,t)$ are the individual jump rates for nucleation, breakage, transport and coagulation, respectively, which are detailed in Section 3.3.

Upon selection of the waiting time, jump process p is carried out with probability

$$\frac{R^{\text{SWA}}_{p}(z,t)}{R^{\text{SWA}}_{\text{total}}(z,t)} \tag{59}$$

and the system moves forward in time. This process is continued until the stopping condition $t \geq t_{\text{stop}}$ is satisfied.

3.2. Splitting scheme

Due to the small size of primary particles relative to large agglomerates within twin-screw devices, the number concentration of these species may differ by several orders of magnitude. In such situations it is unfeasible to solve the primary particle part of the twin-screw population balance problem using a stochastic particle method (unless the primary particle size is significant relative to the mean aggregate size, or in cases where the physical collision rates to be simulated are relatively low). This is due to the fact that the collision jump rates required for significant transfer of mass between the two species becomes too computationally intensive to simulate within reasonable time-scales. For this

reason, the primary particle population balance equation (2) is solved using an implicit ODE solution technique (discussed further in Section 3.4). The use of both stochastic particle and ODE methods to solve different parts of the coupled population balance equations (1) and (2) closely follows the operator splitting technique presented by Celnik et al. [62]. The nature and implementation of the splitting are discussed further in the following sections.

Due to the interaction between individual stochastic particles and the primary particle phase, it is often more convenient to work in terms of the absolute number of primary particles within a given sample volume (as opposed to the number concentration.) Hence, the remainder of the paper will work in terms of primary particle number and $N_{\text{pp}}(z,t)$ is to be understood as the number of primary particles that exist within the sample volume $V_{\text{samp}}(z,t)$ corresponding to physical compartment z at time t.

3.3. Jump processes

The stochastic jump processes associated with the twin-screw population balance model are presented in this section. Since all of the weight transfer functions employed within these jump processes have been shown to converge to the appropriate forms in the un-weighted aggregate PBE (2), the associated weighted population balance equation is not presented here. For details of the various convergence proofs the reader is directed to works [23, 63, 37, 47].

3.3.1. Nucleation

In this work, the nucleation jump involves the inception of particles of the form

$$(z, x_{\text{nuc}}, w_{\text{nuc}}) \tag{60}$$

at rate

$$R_{\text{nuc}}^{\text{SWA}}(z,t) = \begin{cases} \dfrac{R_{\text{drop}}(z,t)V_{\text{samp}}(z,t)}{V_{\text{real}}(z)w_{\text{nuc}}}, & \text{if } z = 1, \\ 0 & \text{otherwise,} \end{cases} \tag{61}$$

where w_{nuc} is the statistical weight of the nucleus particle to be added. Since the nucleation is the only jump process in this work which increases the number of computational particles in the droplet zone ($z = 1$) and transport is the only process which reduces the number of stochastic particle in this zone, the number of particle in $z = 1$ can be held approximately constant by enforcing

$$R_{\text{nuc}}^{\text{SWA}}(z,t) \approx R_{\text{trans}}^{\text{SWA}}(z,t), \tag{62}$$

where $R_{\text{trans}}^{\text{SWA}}(z,t)$ is the transport jump rate in compartment z (detailed in Section 3.3.4).

From (4), (61) and (62) it follows that

$$w_{\text{nuc}}(z,t) = \frac{(\text{LSR})\dot{m}_{\text{feed}} V_{\text{samp}}(z,t)}{v_{\text{drop}}\rho_{\text{l}} V_{\text{real}}(z) R_{\text{trans}}^{\text{SWA}}(z,t)}. \tag{63}$$

3.3.2. Coagulation

Aggregate collision jumps take the following number-conserving form

Coagulating collision:

$$(z, x_i, w_i), (z, x_j, w_j) \mapsto (z, T_{\text{coag}}(x_i, x_j), \gamma_{\text{coag}}(x_i, w_i, x_j, w_j)), (z, x_j, w_j), \tag{64}$$

Non-coagulating collision:

$$(z, x_i, w_i), (z, x_j, w_j) \mapsto (z, x_i, w_i), (z, x_j, w_j), \tag{65}$$

where γ_{coag} is the coagulation weight transfer function. In this work, a mass-conserving form of γ_{coag} is employed - whose convergence has been demonstrated in [63, 23] and has been utilised in previous SWA studies [47, 37]. This has the form

$$\gamma_{\text{coag}}(x_i, w_i, x_j, w_j) = w_i \frac{m(x_i)}{m(x_i) + m(x_j)}. \tag{66}$$

The SWA collision kernel associated with the weight transfer function in (66) is [23]

$$K_{\text{col}}^{\text{SWA}}(z, x_i, w_i, x_i, w_j) = K_{\text{col}}(z, x_i, x_j) w_j \tag{67}$$

$$= k_{\text{col}}(z) n_{\text{screw}} (d_i + d_j)^2 \sqrt{\frac{1}{d_i^3} + \frac{1}{d_j^3}} w_j \tag{68}$$

and the SWA coagulation kernel is

$$K_{\text{coag}}^{\text{SWA}}(z, x_i, w_i, x_i, w_j) = K_{\text{col}}^{\text{SWA}}(z, x_i, w_i, x_i, w_j)\mathbb{1}_{\{x_i, x_j | \text{St}_\text{v}(x_i, x_j) \leq \text{St}_\text{v}^*(x_i, x_j)\}}(x_i, x_j). \tag{69}$$

Due to the complex form of (68), the repeated evaluation of the associated total collision rate in each compartment is very computationally intensive, since it requires looping through each pair of aggregates within the ensemble. For this reason, a majorant kernel is employed. An in-depth treatment of majorant techniques and their application to the solution of population balance problems can be found in [64, 65, 60, 23, 66]. The majorant form of (68) used is

$$\hat{K}_{\text{col}}^{\text{SWA}}(z, x_i, w_i, x_i, w_j) = k_{\text{maj}} k_{\text{col}}(z) n_{\text{screw}} (d_i^2 + d_j^2) \left(\frac{1}{d_i^{1.5}} + \frac{1}{d_j^{1.5}} \right) w_j, \tag{70}$$

where k_{maj} is the majorant scaling factor. As in Lee et al. [47], k_{maj} was set to 1.42 in order to satisfy the inequality $K_{\text{col}}^{\text{SWA}} < \hat{K}_{\text{col}}^{\text{SWA}}$ throughout the simulation.

The majorant collision jump rate in compartment z at time t is (adapted to the current model from [47])

$$\begin{aligned}
R_{z,\,\text{col}}^{\text{SWA}}(z,t) &= \frac{1}{V_{\text{samp}}(z,t)} \sum_{i \neq j}^{N_{\text{agg}}(z,t)} \hat{K}_{\text{col}}^{\text{SWA}}(z, x_i, w_i, x_j, w_j) \\
&= \frac{k_{\text{maj}}\, k_{\text{col}}(z) n_{\text{screw}}}{V_{\text{samp}}(z,t)} \Bigg\{ \left[\sum_{i=1}^{N_{\text{agg}}(z,t)} {d_i}^{0.5} \sum_{j=1}^{N_{\text{agg}}(z,t)} w_j - \sum_{i=1}^{N_{\text{agg}}(z,t)} {d_i}^{0.5} w_i \right] \\
&+ \left[\sum_{i=1}^{N_{\text{agg}}(z,t)} {d_i}^{2} \sum_{j=1}^{N_{\text{agg}}(z,t)} {d_j}^{-1.5} w_j - \sum_{i=1}^{N_{\text{agg}}(z,t)} {d_i}^{0.5} w_i \right] \\
&+ \left[\sum_{i=1}^{N_{\text{agg}}(z,t)} {d_i}^{-1.5} \sum_{j=1}^{N_{\text{agg}}(z,t)} {d_j}^{2} w_j - \sum_{i=1}^{N_{\text{agg}}(z,t)} {d_i}^{0.5} w_i \right] \\
&+ \left[\sum_{i=1}^{N_{\text{agg}}(z,t)} 1 \sum_{j=1}^{N_{\text{agg}}(z,t)} {d_j}^{0.5} w_j - \sum_{i=1}^{N_{\text{agg}}(z,t)} {d_i}^{0.5} w_i \right] \Bigg\}.
\end{aligned} \tag{71}$$

Using the majorant rate expression in (71), jumps are accepted with probability

$$\mathbb{P}_{\text{accept}}(z, x_i, w_i, x_j, w_j) = \frac{K_{\text{col}}^{\text{SWA}}(z, x_i, w_i, x_i, w_j)}{\hat{K}_{\text{col}}^{\text{SWA}}(z, x_i, w_i, x_i, w_j)}, \tag{72}$$

otherwise the jump is fictitious, in which case the ensemble remains unchanged and time moves forward according to (57). Again, the collision pair must satisfy the Stokes criterion in order for the jump to proceed, otherwise the collision is non-coagulating and the system remains unchanged, since the jump (65) has no effect on the system state.

For a full derivation of the majorant rate expression in (71) and the associated particle selection measures, the reader is referred to Lee et al. [47].

3.3.3. Breakage

In this paper, aggregate particles undergo breakage according to the jump [37]

$$(z, x_i, w_i) \mapsto (z, y, \gamma_{\text{frag}}(x_i, w_i, y)), \tag{73}$$

which occurs at rate

$$g_{\text{break}}(z, x). \tag{74}$$

Here, γ_{frag} is the breakage weight transfer function which takes the form [37]

$$\gamma_{\text{frag}}(x_i, w_i, y) = w_i \frac{m(x_i)}{m(y)}. \tag{75}$$

As in [37, 47], convergence is achieved by selecting y according to the following probability measures:

$$\mathbb{P}(y = x_j) = \frac{m(x_j)}{m(x_i)}, \tag{76}$$

$$\mathbb{P}(y = x_i - x_j) = 1 - \frac{m(x_j)}{m(x_i)}. \tag{77}$$

The volume of x_j is selected according to (22) and its composition is that of particle x_i.

The total breakage jump rate in compartment z is

$$R^{\text{SWA}}_{\text{break}}(z, t) = \sum_{i=1}^{N_{\text{agg}}(z,t)} g_{\text{break}}(z, x_i). \tag{78}$$

3.3.4. Transport

Aggregate particle inflow and outflow processes are grouped and carried out under an overarching 'transport' jump process. The transport jump takes the following spatially-dependent forms

1. Droplet zone ($z = 1$)

   Due to the absence of aggregate inflow in to the first reactor, the transport jump only captures outflow through the deletion of a stochastic particle as

$$(z, x, w) \mapsto \text{deleted}. \tag{79}$$

2. Non-droplet zone ($z > 1$)

$$(z, x_i, w_i) \mapsto \text{deleted}, \tag{80}$$

$$(z-1, x_j, w_j) \mapsto (z, x_j, F_{\text{c}}(z,t)w_j). \tag{81}$$

   Here, F_{c} is the transport scaling factor required to maintain continuity, which takes the form

$$F_{\text{c}}(z,t) = \frac{V_{\text{samp}}(z,t)N_{\text{agg}}(z-1,t)}{V_{\text{samp}}(z-1,t)N_{\text{agg}}(z,t)}. \tag{82}$$

   A complete derivation of (82) is provided in Appendix 7.

In all zones, the transport jump is carried out with total rate

$$R^{\text{SWA}}_{\text{trans}}(z,t) = \frac{N_{\text{agg}}(z,t)}{\tau(z)}. \tag{83}$$

3.4. Continuous Processes

Primary particle transport, primary particle depletion through nucleation, layering of primary particles onto stochastic particles (aggregates) and aggregate consolidation are carried out as continuous processes using the Linear Process Deferment Algorithm (LPDA) [44]. LPDA can be thought of as an operator splitting technique with a "just in time" feature. LPDA has been employed in

the simulation of stochastic population balance equations for granulation [37], silica nanoparticle synthesis [38] and soot particle formation [44, 23]. As part of the LPDA, each computational particle is tagged with the time t_p that it has been simulated to. In the LPDA, deferred processes are carried out at two specific stages during the simulation:

1. Local Application

   Here, stochastic particles that are selected to take part in one of the jump processes described in Section 3.3 are brought up to the current simulation time t by applying the aggregate deferment function D_t to each of the selected particles in turn (see Section 2.2.5). This is done just before the jump transforms are applied (i.e."just in time").

2. Global Application

   In these instances, the continuous processes are periodically applied to the full ensemble of stochastic particles between jump processes. This global deferment is carried out with rate $1/\Delta t_\mathrm{defer}$, where Δt_defer is the deferment time step. The global deferment procedure is described in detail in Algorithm 1. Primary particle transport processes are also carried out after each global deferment step (this is discussed further in 3.4.2). The global deferment step ensures that the time over which a particle is integrated is small, such that any linearisations have minimal effect on the solution. This also ensures that the computed jump rates remain close to that of the 'true' undeferred system.

3.4.1. Layering as a deferred process

Since layering is not strictly a linear process (the layering rate for each stochastic aggregate is a function of primary particle concentration), application of the LPDA to the layering processes described in (28)-(31) requires linearisation of the these equations. This is done by assuming that N_pp is approximately constant over the deferment time step. In the context of local deferment, this requires one to hold $N_\mathrm{pp}(z)$ constant while all selected particles are integrated

to the target time. In the context of global deferment steps, the assumption requires one to hold the $N_{\mathrm{pp}}(z)$ constant across each integration interval $\Delta t_{\mathrm{defer}}$ (i.e. all particles are integrated using the same value of $N_{\mathrm{pp}}(z)$ for each global deferment step and $N_{\mathrm{pp}}(z)$ is updated between deferment steps). Such assumptions have been employed using LPDA to describe the surface growth of stochastic particles within the context of soot models [62]. Preliminary simulations with the twin-screw model confirmed that this assumption was appropriate, provided that a small enough deferment time step $\Delta t_{\mathrm{defer}}$ was enforced.

3.4.2. Primary particle update

As mentioned in the previous section, N_{pp} is assumed constant over the course of the deferment step and only updated at the end of each deferment step. These updates take different forms depending on the context in which the deferment is being applied. Let t_{target} denote the time at the end of the deferment step, then the possible forms of primary particle update are

1. Local Application

$$N_{\mathrm{pp}}(z, t_{\mathrm{target}}) \leftarrow N_{\mathrm{pp}}(z,t) - \frac{1}{v_{\mathrm{pp}}} \sum_{i=1}^{N_{\mathrm{p,jump}}} \left[s_{\mathrm{o}}(x_i)_{t_{\mathrm{target}}} - s_{\mathrm{o}}(x_i)_{t_{\mathrm{p}}} \right] w_i, \quad (84)$$

where $N_{\mathrm{p,jump}}$ is the number of particle involved in the selected jump process and the second term on the RHS represents the linearised SWA form of the final (layering) term in (2), taken over only the particle(s) involved in the local deferment. The derivation of this term is provided in Appendix 8.

2. Global Application

$$\begin{aligned} N_{\mathrm{pp}}(z, t_{\mathrm{target}}) \leftarrow & N_{\mathrm{pp}}(z,t) \\ & - \frac{1}{v_{\mathrm{pp}}} \sum_{i=1}^{N_{\mathrm{agg}}(z,t)} \left[s_{\mathrm{o}}(x_i)_{t_{\mathrm{target}}} - s_{\mathrm{o}}(x_i)_{t_p} \right] w_i \\ & + (t - t_{\mathrm{target}}) \left. \frac{\mathrm{d}N_{\mathrm{pp}}(z,t)}{\mathrm{d}t} \right|_{\mathrm{transport}} \\ & + (t - t_{\mathrm{target}}) I^{\mathrm{nuc}}_{t,\mathrm{pp}}(z) V_{\mathrm{samp}}(z,t). \end{aligned} \quad (85)$$

The second term on the RHS of (85) is the same as the local case (84), except that the layering term has been integrated across the full ensemble of stochastic particles in compartment z. The third term on the RHS of (85) represents the integral of the linearised primary particle transport rate (Equation (43)), which, applied to the network of sample volumes, takes the form

$$\left.\frac{\mathrm{d}N_{\mathrm{pp}}(z,t)}{\mathrm{d}t}\right|_{\mathrm{transport}} = \begin{cases} \dfrac{\dot{m}_{\mathrm{feed}} V_{\mathrm{samp}}(z,t)}{V_{\mathrm{real}}(z)\rho_s v_{\mathrm{pp}}} - \dfrac{N_{\mathrm{pp}}(z,t)}{\tau(z)}, & \text{if } z = 1, \\ \dfrac{V_{\mathrm{real}}(z-1)}{V_{\mathrm{real}}(z)} \dfrac{V_{\mathrm{samp}}(z)}{V_{\mathrm{samp}}(z-1)} \dfrac{N_{\mathrm{pp}}(z-1,t)}{\tau(z-1)} - \dfrac{N_{\mathrm{pp}}(z,t)}{\tau(z)}, & \text{otherwise.} \end{cases} \tag{86}$$

A full derivation of (86) is provided in Appendix 9.

Finally, the last term in (85) is the integral of the nucleation depletion term (43), scaled according to the sample volume.

3.5. Solver implementation

In this paper, the steady state solution of the twin-screw population balance problem described by Equations (1)-(2) is of primary interest. As such, this permits the compartment network to be solved in a sequential manner, starting from $z = 1$ and moving along the network in a linear fashion until the final reactor with $z = \max \mathbb{L}$ is reached. This dramatically reduces the computational effort required to achieve converged solutions, to the extent that large-scale parameter estimation procedures become possible. Since the networks studied here are strictly linear (i.e. no back-flow or recycle loops) a single pass of the network is sufficient to fully converge the compartmental network. Algorithm 2 is a simplified account of the sequential solver algorithm used to solve the twin-screw population balance problem in this study. Preliminary twin-screw simulations using the model presented in this paper and previous twin-screw SWA works [42, 43] showed that, if the initial state of each compartment (i.e. at $t = 0$) has an overall particle concentration that is sufficiently

close to the solution of the population balance problem, then the simulation time required to reach steady state is determined by the residence time of the compartment in question. In this paper, the steady state solution to the population balance problem is defined as the state of the ensemble which does not exhibit any dynamic drift in the key measures (particle moments, overall mass density, mean porosity, liquid content, etc.). Thus each compartment is solved to time

$$t_{\text{stop}}(z) = n_\tau \tau(z), \tag{87}$$

where $n_\tau \in \mathbb{R}^+$. The choice $n_\tau = 8$ was observed to yield simulation stop times that were long enough to reach steady state. Since the reactors are solved in sequence, the transport terms that have a dependence on the previous reactor (such as $N_{\text{agg}}(z-1,t)$) should be replaced with the equivalent steady state value (in this example $N_{\text{agg}}(z-1, t_{\text{stop}}(z-1))$).

Algorithm 1: The global deferment algorithm used to carry out continuous processes, applied to compartment z.

START

if $t == 0$ **then**
  Set $t_{\text{next-defer}} \leftarrow \Delta t_{\text{defer}}$.

while $t_{\text{next-defer}} < t$ **do**
  Integrate all aggregate particles to required time in stages.
  Set $t_{\text{target}} \leftarrow \min\{t_{\text{next-defer}}, t\}$.
  for $i = 1, N_{\text{agg}}(z,t)$ **do**
    Numerically integrate particle (x_i, w_i) to t_{target} according to Equation (42).
  Update $N_{\text{pp}}(z)$ to t_{target} according to (85).
  Set $t_{\text{next-defer}} \leftarrow t_{\text{next-defer}} + \Delta t_{\text{defer}}$.

STOP

Algorithm 2 is applied numerous times (each time with a different seed to the random number generator) in order to generate multiple independent measures of the steady state solution to the twin-screw population balance problem. From here on, each repetition of the algorithm for a fixed set of operating conditions will be referred to as a realisation.

The first compartment is initialised such that 50% of the steady state mass hold-up is allocated to aggregate phase in the form of particles with $x = (v_{\text{drop}}, 0, 0, 0), w = 1$. The remaining mass specifies $N_{\text{pp}}(1, 0)$. In each realisation, the first compartment is initialised with $N_{\text{agg}}(1, 0) = 0.75 N_{\text{agg}}^{\max}$, where

Algorithm 2: The SWA sequential solver algorithm for a single realisation.

START

Set $z = 1$.

while $z \leq \max \mathbb{L}$ **do**

  Set $t \leftarrow 0$.

  Compute $t_{\text{stop}}(z)$ from (87).

  Initialise particle ensemble and $N_{\text{pp}}(z, 0)$.

  while $t < t_{\text{stop}}(z)$ **do**

    Apply global deferment Algorithm (1).

    Compute $R_{\text{total}}^{\text{SWA}}(z, t)$ according to (58).

    Compute Δt_{wait} according to (57).

    Set $t \leftarrow t + \Delta t_{\text{wait}}$.

    Select jump process according to (59).

    Apply local deferment transformation D_t to the selected particle(s).

    Update the particle ensemble according to the selected jump process.

  Set $z \leftarrow z + 1$.

STOP

$N_{\text{agg}}^{\max}$ is the maximum number of computational particles permitted (per compartment). In all subsequent compartments, the particle ensemble and $N_{\text{pp}}(z, 0)$ are initialised with the final state of particle ensemble and N_{pp} in the previous compartment $(z-1)$. The particle doubling and reduction procedures described in Lee et al. [37] are employed to control the number of computational particles in each compartment. Note that this is only important in the case of $z = 1$, since it is the only compartment where inflow and outflow processes are not directly coupled (the coagulation, breakage and non-droplet zone transport jump processes presented in Section 3.3 are all constant number).

4. Application

4.1. Twin-screw operating conditions

The predictive abilities of the twin-screw model are assessed using a two-step process. Firstly, unknown model parameters are estimated using data from selected experiments carried out by Vercruysse et al. [8]. In the second stage, these parameter estimates are used in the simulation of additional experiments by Vercruysse et al. [8], that were not featured in the estimation stage. In the experimental work used, the authors investigated the effect of the screw configuration on the product particle size distribution (PSD) using a ConsiGma$^{\text{TM}}$ twin-screw granulator (length-to-diameter ratio of 20:1) with α-lactose monohydrate as the feed material and distilled water as the binding liquid. The authors tested a large number of screw configurations with slight permutations in the number of specific element types, number of blocks (i.e groups of the same element type) of certain element types, with all other controllable operating conditions fixed. In order to better understand the role of the most common element types (conveying and kneading), only screw configurations that consisted of a combination of kneading and conveying elements (and for which product PSD were presented) were simulated here. The simulated screw configurations and their corresponding compartmental representations are outlined in Figure 5.

Details of the model parameters corresponding to the experimental conditions in Vercruysse et al. [8] are presented in Table 2.

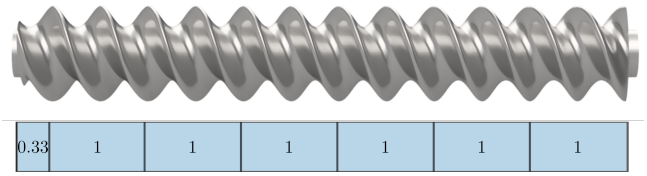

(a) CE

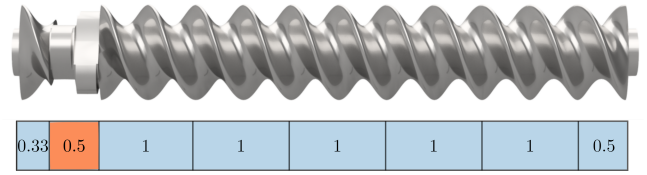

(b) 2KE

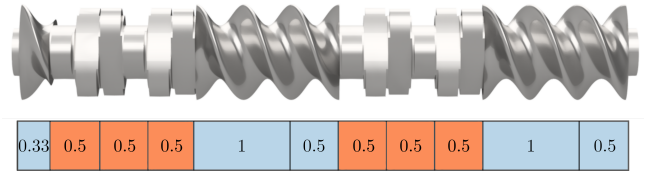

(c) 2x6KE

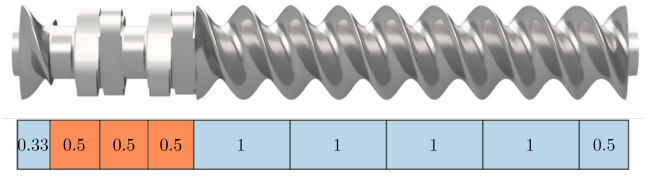

(d) 6KE

Figure 5: Screw configurations modelled in this work and their respective compartmental representations. The number in the centre of each compartment represents the compartment length (normalised by the screw diameter). Compartments representing conveying zones are in blue and compartments representing kneading zones are shown in orange. These correspond to configurations A, B, D and E in Vercruysse et al. [8]

Table 2: Un-optimised model inputs.

Parameter (symbol)	Type	Value	Unit
Liquid:solid mass feed ratio (LSR)	Operating parameter	0.09	-
Mass feed rate ($\dot{m}_{\text{feed}}$)	Operating parameter	20.0	kg hr^{-1}
Screw speed (n_{screw})	Operating parameter	13.33	rev s^{-1}
Screw residence time (τ_{screw}) (CE,2KE,6KE,2x6KE) [49]	Operating parameter (interpolated)	0.753, 3.02, 3.09, 4.52	s
Liquid addition nozzle diameter (d_{nozzle})	Equipment geometry	1.6	mm
Screw diameter (D)	Equipment geometry	25	mm
Specific available volume CE (ν_{convey})	Equipment geometry	1.218×10^{-5}	m^3/D
Specific available volume KE (ν_{knead})	Equipment geometry	1.284×10^{-5}	m^3/D
Coefficient of restitution (e_{coag}) [67]	Material property	0.2	-
Liquid binder viscosity (μ_{binder})	Material property	10^{-3}	Pa s
Liquid binder density (ρ_{l})	Material property	998	kg m^{-3}
Solid original density (ρ_{s})[68]	Material property	1545	kg m^{-3}
Height of surface asperities (h_{a})	Material property (estimated)	5×10^{-6}	m
Representative volume mean primary particle diameter d_{pp}	Material property	27.3	μm
Droplet diameter (d_{drop})	Model parameter	1.6	mm
Minimum particle size for breakage ($v_{\text{parent}}^{\text{min}}$)	Model parameter	27.3	μm
Daughter distribution parameter 1 (α_{daughter}) (CE,KE)	Model parameter	0.5, 2.0	-
Daughter distribution parameter 2 (β_{daughter}) (CE,KE)	Model parameter	0.5, 2.0	-
Minimum particle porosity (ε_{min})	Model parameter	0.3	-
Particle bed packing fraction (ε_{bed})	Model parameter	0.3	-
Pore saturation limit for nucleation (s^*)	Model parameter	0.12	-

Table 3: Numerical input parameters.

Parameter	Value	Unit
$N_{\text{agg}}^{\max}$	1024	-
Δt_{defer}	10^{-4}	s
$n_{\text{realisation}}$	10	-
n_{τ}	8	-
k_{maj}	1.42	-

4.2. Simulation conditions

All simulations were carried out using the numerical inputs given in Table 3 on a single core of an Intel® Sandy Bridge™ E5-2670 3.30GHz Processor with 4GB of RAM per core. Temporal functionals $M(t)$ from the simulations are reported as averages taken over all realisations as

$$\eta(t) = \frac{1}{n_{\text{realisations}}} \sum_{i=1}^{n_{\text{realisations}}} M_i(t), \tag{88}$$

where the functional may be a particle ensemble property such as the mass fraction of particles in a particular sieve class.

The half-width of the confidence intervals are

$$c(t) = 1.64 \sqrt{\frac{\sum_{i=1}^{n_{\text{realisations}}} (M_i(t) - \eta(t))^2}{n_{\text{realisations}}^2}}, \tag{89}$$

which corresponds to a confidence interval $P = 0.9$ [37].

4.3. Parameter estimation

In this work, compartments with the same element type (conveying, kneading) are assumed to have the same process rate constants (4 for each element type, 8 in total), regardless of position. In this way, a central screw element library can be used to store element specific rate constants. This library can then be accessed to retrieve and define the rate constants for each compartment in an representation of arbitrary screw configurations. Using this framework, the model can be calibrated against experimental data through the optimisation of the relevant variables in the screw element library. The procedure for

optimising each of the variables within the screw element library follows that described in McGuire et al. [42] and is only described briefly here for clarity. The rate constants are fitted against experimental data [8] corresponding to screw configurations CE, 2KE and 2x6KE (see Figure 5). Screw configuration 6KE is then used to measure the predictive power of the model. An initial parameter scan is carried out using 10000 Sobol points [69] across the parameter ranges outlined in Table 4. A Hooke Jeeves optimisation [70] is then carried out using the best 4 Sobol points from the first optimisation step as the starting positions. Both stages are carried out using the Model Development Suite (MoDS) [71]. The objective function used in the fitting takes the form

$$OF = \sum_{i=1}^{N_{\text{exp}}} \sum_{j=1}^{N_{\text{response}}} \left(\frac{y_{j,i}^{\text{model}} - y_{j,i}^{\text{exp}}}{\sigma_j} \right)^2 . \tag{90}$$

Here, $y_{i,j}^{\text{model}}$ is the j^{th} model response for the i^{th} screw configuration modelled and $y_{j,i}^{\text{exp}}$ is the associated experimental response. N_{exp} is the number of different screw configurations fitted and N_{response} model/experimental responses from each configuration. Mass based percentiles diameters d25, d50, d75 and d95 of the granular product in [8] are used as the model/experimental responses. These are weighted, respectively, using weighting factors σ of 25μm, 50μm, 75μm and 95μm.

Table 4: Bounds used for optimisation of model parameters.

	Conveying		Kneading			
Parameter	Lower	Upper	Lower	Upper	Scaling	Unit
k_{col}	10^{-10}	5×10^{-8}	10^{-10}	2×10^{-8}	Logarithmic	$\text{m}^{\frac{5}{2}}$
k_{comp}	10^{-2}	2.0	10^{-2}	2.0	Logarithmic	-
k_{att}	1.68×10^{-2}	8.4	1.68×10^{-3}	0.0168	Logarithmic	s
ω_{att}	10^{-2}	0.2	5×10^{-2}	0.6	Linear	-

Table 5: Optimised model rate constants with OF=753.8.

Parameter	Conveying	Kneading	Unit
k_{col}	10^{-10}	2.0×10^{-8}	$\text{m}^{\frac{5}{2}}$
k_{comp}	0.01	0.475	-
k_{att}	0.0168	9.358×10^{-3}	s
ω_{att}	0.1095	0.387	-

5. Model results

The set of model parameters with the lowest objective function value (found through the optimisation procedure) are presented in Table 5. The associated mass fraction distributions for this parameter set are displayed, firstly, for screw configurations used in the optimisation procedure in Figure 6, and secondly, for the 'new' 6KE screw configuration (depicted in Figure 5(c)) in Figure 7.

Note that the model has qualitatively captured the experimental trend in which the amount of fines (defined here as particles in the smallest sieve class) reduces with an increasing number of kneading elements. This is expected since the kneading elements serve to distribute the binding liquid across the body of solid material passing through the element, thereby promoting particle growth. Though the model has captured this trend, the degree of primary particle consumption is under-predicted for all screw configuration tested - thought the disparity in minimal in the 2x6KE case. This is to be expected since a very simplistic layering mechanism was employed in this work. Within the model, the degree of layering is strongly controlled by the amount of surface liquid present on agglomerates, however, the amount of surface liquid that should be consumed by layering is unclear and hence a very basic model has been used. Implementation of more complex models in the future would require experimental data on the layering dynamics in isolation from other twin-screw processes.

In terms of breakage processes, the model has under-predicted the production of particles in the size range 200-1000μm in screw elements with a high

number of conveying elements. This is an indication that the breakage parameters that generate this distribution (daughter distribution shape parameters α_{daughter}, β_{daughter} and breakage exponent ω_{att}) may need to be revisited. As previously discussed, the daughter distribution parameters used for conveying elements in this work were selected to qualitatively capture the cutting and edge chipping effects that were experimentally observed in such elements. Since these parameters were not fitted within this study, it is likely that these parameters would benefit from further investigation. This would merit a modelling investigation in its own right and is not pursued further here. It is noted that the compaction, breakage and coagulation processes have all been pushed to their lower bound as a result of the optimisation process. This indicates that the majority of the model particle processes occurred in the kneading elements. The bounds of these conveying parameters were not reduced further, since the effect on the results was deemed to be minimal. Note that the kneading element collision rate has also been pushed to its upper bound in the parameter estimation process, bringing the total number parameters at their bounds to four. This result is likely a combination of a number of factors. Firstly, even though the best Sobol point identified in the first stage of the parameter estimation may be well within the bounds of the space, the additional Hooke-Jeeves local optimisation stage on these points often pushes one or more parameters to their bounds. Due to the high computational cost of the combined stages, it is computationally prohibitive to iterate this process any significant number of times to ensure that the bounds yield both particle evolutions that both plausible and that all optimised parameters lie within their bounds. All of the parameters that have hit their lower limit are associated with the conveying zone. This is likely due to the lower residence time in the conveying zone associated with the conveying zone relative the kneading elements. It should also be noted that the configuration of kneading elements in the screw configuration modelled (Figure 5) are not angled at 90^o to each other. This means that they will have some conveying capacity and hence will not be completely filled with material as assumed in the residence time model. Taking this in account would reduce the

kneading element residence time estimates and thereby increase the residence times estimates for the conveying zones. Alternatively, to ensure parameters in the conveying zone carry more weight in the optimisation process, mid-barrel PSD data would need to be measured and integrated into the objective function of the optimisation process. At the moment, only the final distribution is in this process, which can lead to un-physical particle evolutions or concentration of particle processes in distinct sections, as observed here.

The evolution of the particle size distribution and key percentile diameters along the compartmental networks are shown for the 2x6KE screw configuration in Figure 8 and Figure 9, respectively. The nucleation zone consists of a mixture of over-sized agglomerates and primary particle mass. Upon entering the first kneading compartment ($z = 2$, barrel position 0.09) these large agglomerates are broken down and consolidated. The consolidation process has resulted in the squeezing of internal liquid to the particle surface which has promoted consumption of fines through layering. This trend continues through the second and third kneading compartment. It is clear from the both Figure 8 and Figure 9 that there is little change in the granular mass as it passes through the central conveying section ($z = \{6, 7\}$ barrel position 0.48 - 0.57). Only a minimal degree of breakage is observed in this zone, and, as discussed in the previous paragraph, the absence of the expected increase in intermediate size classes (200-400μm) for the 2x6KE simulation indicates that the daughter distribution of these elements requires further investigation. Almost all of the remaining fines are consumed within the second kneading section of the compartment network, resulting in an increase in all percentile diameters in Figure 9.

In order to further assess the quality of the model, the evolution of the agglomerate particle composition along the screw barrel for each simulated screw configuration is presented in Figure 10. The associated mass fraction of fines at each of the these barrel positions, in each screw configuration, is shown in Figure 11. From Figure 10 it is observed that, for the conveying elements, a slight degree of particle compaction has reduced the porosity of large agglomerate particles, which resulted in the complementary increase in solid volume

fraction. Though the solid volume fraction increase could be attributed to particle growth through layering and coagulation, the minimal fines consumption for the CE configuration in Figure 11 and the abundance of surface liquid in Figure 10 (which should promote aggregate coagulation if the collision rate is sufficiently high) demonstrates that this is almost purely the result of aggregate compaction. In all configurations with a kneading zone, it is observed that, for the first kneading zone, aggregate particles acquire solid mass though the consolidation of highly porous agglomerates. This consolidation has replenished surface liquid levels, which promoted layering of primary particles and coalescence of surface wet agglomerates. This decrease in surface liquid observed in Figure 10 is a consequence of the internalisation of liquid present in both the aggregate consolidation and primary particle layering mechanisms of the model. This raises an interesting point - though several experimental studies [11, 72, 73, 74, 8] have concluded that kneading elements squeeze liquid to the surface of large agglomerates, promoting further growth, it is generally not understood if this growth takes place within the kneading element, or further down the barrel in conveying zones. From Figure 11, the model in this work would seem to indicate that the majority of this growth and fines reduction occurs within the kneading blocks.

An interesting feature that is observed in particle evolution of the 2x6KE screw configuration is the increase in gas volume fraction within the second kneading block. This occurred as the result of aggregate coalescence - which, according to the coalescence model of Braumann et al. [30] used in this work, results in the generation of trapped pore volume as aggregates coalesce. Though trapping of such 'new' pore volume may occur, it is expected that a net reduction in porosity would be observed across this kneading block (as is the case in the first kneading block of all screw configurations tested). Thus, the competition between the consolidation forces and pore volume creation through coalescence would be an area of investigation in future modelling efforts.

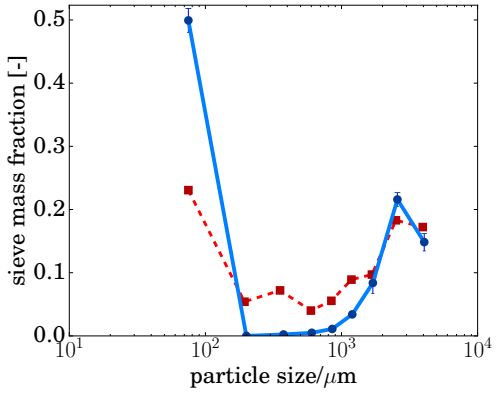

(a) CE

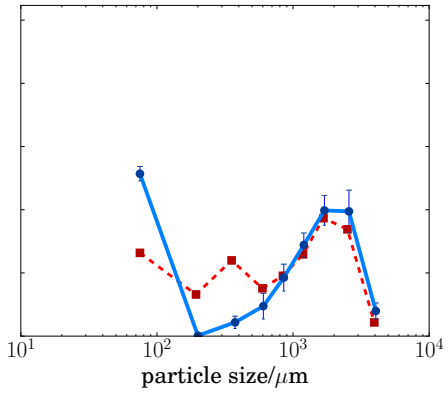

(b) 2KE

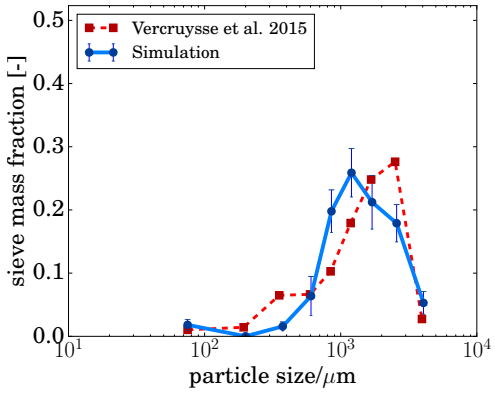

(c) 2x6KE

Figure 6: A comparison of the optimised model particle size distributions in the final compartment against the experimental results from Vercruysse et al. [8] for different screw configurations.

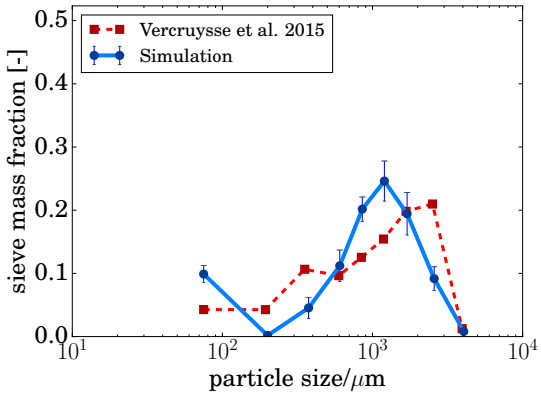

Figure 7: A comparison of simulated and experimental results (Vercruysse et al. [8]) using optimised model rate constants for a 6KE screw configuration (not used in the optimisation stage).

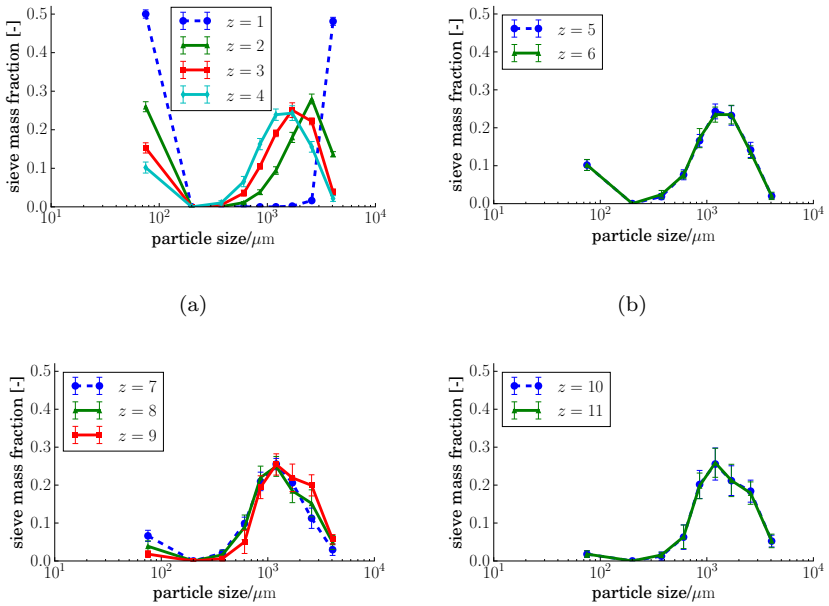

Figure 8: Particle size distribution evolution along the compartment network for the 2x6KE screw configuration. Element types by compartment index: conveying $z = \{1, 5, 6, 10, 11\}$, kneading $z = \{2, 3, 4, 7, 8, 9\}$.

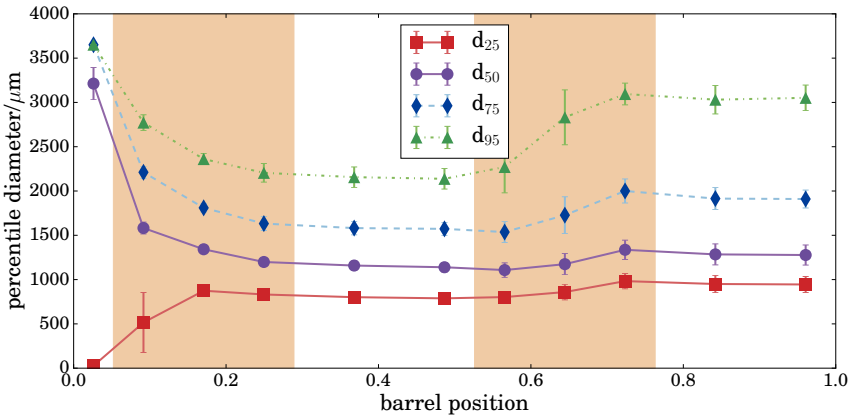

Figure 9: Mass-based percentile diameter evolutions along the barrel length for the 2x6KE screw configuration. Kneading zones are highlighted in orange. Data points are placed according to the centre of the associated compartment. Barrel positions correspond to the variation zone and are expressed as a normalised length.

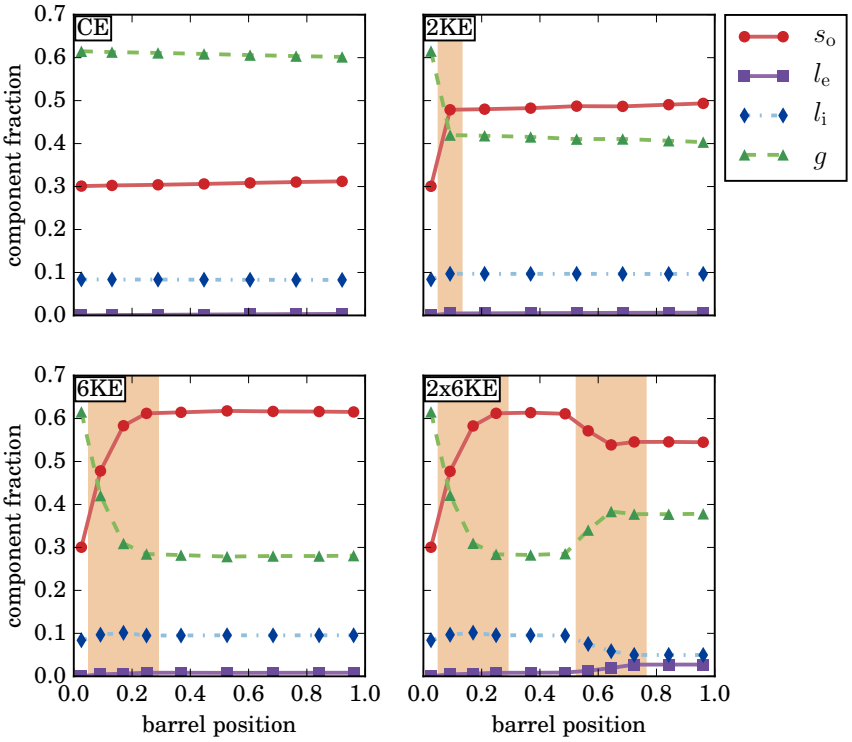

Figure 10: Mass-averaged aggregate particle composition evolutions (by volume) along the barrel length for each screw configuration simulated. s_o represents original solid, l_e represents external liquid, l_i represents internal liquid and g is gas. Kneading zones are highlighted in orange. Data points are placed according to the centre of the associated compartment. Barrel positions correspond to the variation zone and are expressed as a normalised length.

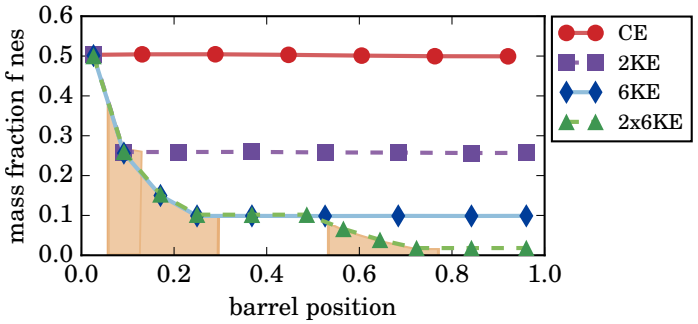

Figure 11: Simulated evolution of the mass fraction of fines (d $< 75\mu$m) along the length of the barrel for all screw configurations tested. Data points are placed according to the centre of the associated compartment. Barrel positions correspond to the variation zone and are expressed as a normalised length. Kneading zones are highlighted in orange.

6. Conclusions

In this work, the twin-screw granulation model of [42, 43] has been adapted and extended to include a primary particle layering mechanism and a screw element-dependent breakage model. In order to estimate compartmental residence times for use within this model, a novel procedure was developed to infer this parameter based on the type of screw element associated with each compartment. A stochastic particle framework for the simulation of the aggregate particle phase of the granulation system was presented and coupled to an ODE solver in order to simulate the dynamics of the primary particle population and carry out continuous aggregate particle processes. Model parameters specific to different types of screw element were calibrated through simulation of systems with a number of different screw configurations and comparison with an existing experimental data set. The model was observed to qualitatively capture the reduction in the mass fraction of fines in the granular product as the number of kneading elements was increased, however, the model over-predicted the amount of fines in the product for all but the 2x6KE screw configuration. It was shown that the optimised model was able to predict the PSD of the twin-screw granular product at large particle diameters with reasonable accuracy, for various screw configurations. The element specific breakage model and the drying dynamics of the layering process were identified as key areas for future model refinement.

Acknowledgements

ADM acknowledge funding from EPSRC Grant 1486478 and AstraZeneca. ADM would also like to thank C. T. Lao for useful conversations regarding the implementation of the nucleation process. RP acknowledges support from the Deutsche Forschungsgemeinschaft (DFG) through grant CRC 1114 "Scaling Cascades in Complex Systems", Project C08. This project was partly funded by the National Research Foundation (NRF), Prime Minister's Office, Singapore under its Campus for Research Excellence and Technological Enterprise (CREATE) programme.

Abbreviations

CE	Conveying element
DEM	Discrete element method
DME	Distributive mixing element
KE	Kneading element
LPDA	Linear process deferment algorithm
PBE	Population balance equation
PBM	Population balance model
PEPT	Positron emission particle tracking
MC-PBM	Monte Carlo population balance model
SWA	Stochastic weighted algorithm
TSG	Twin-screw granulation

Nomenclature

Roman symbols

a_{surf}	particle external surface area	m^2
B_{frag}	breakage fragment probability distribution	-
c_{pp}	primary particle concentration measure	m^{-3}
C	collision rate function	$\text{m}^{\frac{1}{2}}$
d	particle diameter	m
d_{nozzle}	liquid injection nozzle diameter	m
d_{pp}	primary particle diameter	m
D_t	deferment function	-
e_{coag}	material coefficient of restitution	-
f_{frag}	breakage fragment size parameter	-
$f_{\text{j,e}}$	volumetric fill fraction of screw section with element type e in zone j	-
F	aggregate breakage kernel	-
F_{c}	transport scaling factor	-
g	particle gas volume	m^3
g_{break}	particle breakage frequency	s^{-1}
h_{a}	height of surface asperities	m
h_{l}	height of external liquid layer	m
$I_{\text{nuc,pp}}$	primary particle depletion sink term (nucleation)	$\text{s}^{-1}\text{m}^{-3}$
$I_{\text{trans,pp}}$	primary particle depletion source term (transport)	$\text{s}^{-1}\text{m}^{-3}$
k_{att}	attrition rate constant	s
k_{col}	collision rate constant	$\text{m}^{\frac{5}{2}}$
k_{comp}	compaction rate constant	-
k_{maj}	majorant scaling factor	-
K_{coag}	coagulation kernel	m^3s^{-1}

$K_{\text{coag}}^{\text{SWA}}$	SWA coagulation kernel	m^3s^{-1}
K_{col}	collision kernel	m^3s^{-1}
$\hat{K}_{\text{col}}$	collision kernel term	m^3s^{-1}
$K_{\text{col}}^{\text{SWA}}$	SWA collision kernel	m^3s^{-1}
$\hat{K}_{\text{col}}^{\text{SWA}}$	SWA majorant collision kernel	m^3s^{-1}
l_{e}	external liquid volume	m^3
$l_{\text{e}\rightarrow\text{i}}$	amount of surface liquid internalised	m^3
l_{i}	internal liquid volume	m^3
$L_{\text{j,e}}$	length of screws section consisting of element type e in zone j	D
$\mathbb{L}$	set of all compartment indices	-
LSR	operating liquid solid mass flowrate ratio	-
m	particle mass	kg
$\dot{m}_{\text{feed}}$	operating mass feed rate	kg s^{-1}
M_{metering}	dynamics mass hold up in screw metering zone	kg
$M_{\text{variation}}$	dynamics mass hold up in screw variation zone	kg
$n_{\text{realisations}}$	number of simulation realisations	-
n_{screw}	screw speed	rev s^{-1}
n_{τ}	simulation stop time parameter	-
N_{agg}	number of aggregate/computational particles	-
$N_{\text{agg}}^{\text{max}}$	maximum number of aggregate/computational particles	-
N_{pp}	Number of primary particles	-
OF	objective function	-
p	pore volume	m^3
r_{inflow}	single particle inflow rate	s^{-1}
r_{layer}	rate of primary particle layering onto agglomerate particle	s^{-1}
R_{drop}	model droplet addition rate	s^{-1}
R_{nuc}	model nucleation rate	s^{-1}

$R_{\text{outflow,agg}}$	model aggregate outflow rate	s^{-1}
$R_{\text{break}}^{\text{SWA}}$	SWA breakage jump rate	s^{-1}
$R_{\text{coag}}^{\text{SWA}}$	SWA coagulation jump rate	s^{-1}
$R_{\text{nuc}}^{\text{SWA}}$	SWA nucleation jump rate	s^{-1}
$R_{\text{total}}^{\text{SWA}}$	SWA total jump rate	s^{-1}
$R_{\text{trans}}^{\text{SWA}}$	SWA transport jump rate	s^{-1}
s_{o}	original solid volume	m^3
s^*	pore saturation limit	-
t	time	s
t_{p}	particle current time	s
t_{stop}	simulation stop time	s
t_{target}	deferment stop time	s
Δt_{wait}	jump waiting time	s
Δt_{defer}	deferment time step	s
T_{coag}	coagulation type transformation	-
v	particle volume	m^3
$\hat{v}_{\text{break}}$	breakage normalisation parameter	m^3
$v_{\text{parent}}^{\text{min}}$	minimum volume for breakage	m^3
v_{pp}	primary particle volume	m^3
v_y	breakage daughter volume function	m^3
V_{real}	physical volume of compartment occupied by mass	m^3
V_{samp}	sample volume	m^3
w	particle statistical weight	-
w_{max}	maximum particle statistical weight	-
w_{nuc}	nuclei particle statistical weight	-
x	particle vector	m^3
x_{nuc}	nuclei particle vector	-

x_{pp}	primary particle vector	-
$\mathbb{X}$	particle type-space	-
$\mathbb{X}_{\text{agg}}$	aggregate type-space	-
$\mathbb{X}_{\text{pp}}$	primary particle type space	-
y	breakage fragment particle vector	m^3
z	compartment index	-

Greek symbols

α_{daughter}	breakage daughter distribution shape factor	-
β_{daughter}	breakage daughter distribution shape factor	-
γ_{coag}	coagulation weight transfer function	-
γ_{frag}	breakage weight transfer function	-
ε	particle porosity	-
ε_{bed}	particle bed packing fraction	-
λ	aggregate particle concentration measure	m^{-3}
ν_{convey}	specific volume available in conveying elements	m^3/D
ν_{knead}	specific volume available in kneading elements	m^3/D
ν_{convey}	specific volume available in conveying elements	m^3/D
ρ_{eff}	effective density of the solid material in the variation zone	kg m^{-3}
ρ_{l}	binder density	kg m^{-3}
ρ_{s}	solid density	kg m^{-3}
ϕ_{max}	maximum liquid saturation	-
σ	objective function weighting factor	μm
τ	compartment residence time	s
τ_{metering}	metering zone screw residence time	s
τ_{screw}	total mean screw residence time	s
$\tau_{\text{variation}}$	variation zone screw residence time	s

χ_{frag}	breakage fragment size parameter	-
φ	test function	-
ω_{att}	breakage rate exponent	-

7. Appendix: derivation of transport scaling factor

It is desired to show that the weight scaling factor applied to inflow particles within the transport jump process (81) has the form:

$$F_{\mathrm{c}}(z,t) = \left[\frac{V_{\mathrm{samp}}(z,t)}{V_{\mathrm{samp}}(z-1,t)}\right]\left[\frac{N_{\mathrm{agg}}(z-1,t)}{N_{\mathrm{agg}}(z,t)}\right]. \tag{91}$$

in the context of a non-droplet zone compartment ($z \neq 1$) for a twin-screw model system.

Firstly, it is asserted that each compartment in the network is one of constant mass and volume (i.e $M_{\mathrm{real}}(z), V_{\mathrm{real}}(z) \neq f(t)$ and thus, to provide continuity, the mass flow rate through each compartment $\dot{m}_{\mathrm{feed}}$ is the same). It follows that concentration of mass flow entering/leaving the sample volume (denoted by the superscript $^{\mathrm{SV}}$) for compartment z must be the same as that entering the physical system i.e.

$$\frac{\dot{m}^{\mathrm{SV}}_{\mathrm{inflow}}(z,t)}{V_{\mathrm{samp}}(z)} = \frac{\dot{m}^{\mathrm{SV}}_{\mathrm{outflow}}(z,t)}{V_{\mathrm{samp}}(z,t)} = \frac{\dot{m}_{\mathrm{feed}}}{V_{\mathrm{real}}(z)} \tag{92}$$

Thus, the mass flow of aggregate particles entering the sample volume can be related to the mass fraction of aggregates (in a mixture of aggregates and primary particles) in the preceding compartment (at steady state) as

$$\dot{m}^{\mathrm{SV}}_{\substack{\mathrm{agg,inflow}\\ z\in\mathbb{L},\ z>1}}(z,t) = \dot{m}^{\mathrm{SV}}_{\mathrm{inflow}}(z,t)\frac{M^{\mathrm{SV}}_{\mathrm{agg}}(z-1,t)}{M^{\mathrm{SV}}_{\mathrm{total}}(z-1,t)} \tag{93}$$

$$= \frac{\dot{m}_{\mathrm{feed}} M^{\mathrm{SV}}_{\mathrm{agg}}(z-1,t) V_{\mathrm{samp}}(z,t)}{V_{\mathrm{real}}(z) M^{\mathrm{SV}}_{\mathrm{total}}(z-1,t)}, \tag{94}$$

where $M^{\mathrm{SV}}_{\mathrm{agg}}(z,t)$ and $M^{\mathrm{SV}}_{\mathrm{total}}(z,t)$ are the mass of aggregates and the total mass (primary particles and aggregates) in the sample volume, respectively.

Let the number average mass of computational particles (aggregates) in the sample volume associated with compartment z be defined as

$$\langle mw \rangle_{z,t} := \frac{M^{\mathrm{SV}}_{\mathrm{agg}}(z,t)}{N_{\mathrm{agg}}(z,t)}. \tag{95}$$

It is required that the inflow process to compartment z sample the particle distribution from compartment $z-1$. Thus, the weights of particles sampled

from the preceding reactor can be freely scaled by some constant scaling factor F_{c}, prior to their inception into the current reactor. This scaling has no effect on the physical particle distribution in compartment $z-1$. Incorporating this scaling factor, the average mass of a particle incepted into compartment z from compartment $z-1$ during an inflow event is

$$F_{\mathrm{c}}\langle mw\rangle_{z-1,t}. \tag{96}$$

The mass inflow rate into compartment z may be written in an alternative form, which is based on the rate of inflow events $R^{\mathrm{SWA}}_{\mathrm{inflow}}(z,t)$ as

$$\underset{z\in\mathbb{L},\ z>1}{\dot{m}^{\mathrm{SV}}_{\mathrm{agg,inflow}}}(z,t) = R^{\mathrm{SWA}}_{\mathrm{inflow}}(z,t)F_{\mathrm{c}}\langle mw\rangle_{z-1,t}. \tag{97}$$

Equating (94), (97) and substituting (95), yields

$$\underset{z\in\mathbb{L},\ z>1}{R^{\mathrm{SWA}}_{\mathrm{inflow}}}(z,t) = \frac{\dot{m}_{\mathrm{feed}}V_{\mathrm{samp}}(z,t)N_{\mathrm{agg}}(z-1,t)}{V_{\mathrm{real}}(z)M^{\mathrm{SV}}_{\mathrm{total}}(z-1,t)F_{\mathrm{c}}}. \tag{98}$$

Using the residence time definition

$$\dot{m}_{\mathrm{feed}} := \frac{M_{\mathrm{real}}(z-1)}{\tau(z-1)} \tag{99}$$

$$= \frac{M^{\mathrm{SV}}_{\mathrm{total}}(z-1,t)V_{\mathrm{real}}(z-1)}{\tau(z-1)V_{\mathrm{samp}}(z-1,t)}, \tag{100}$$

(98) may be written as

$$\underset{z\in\mathbb{L},\ z>1}{R^{\mathrm{SWA}}_{\mathrm{inflow}}}(z,t) = \left[\frac{V_{\mathrm{real}}(z-1)}{V_{\mathrm{real}}(z)}\right]\left[\frac{V_{\mathrm{samp}}(z,t)}{V_{\mathrm{samp}}(z-1,t)}\right]\left[\frac{N_{\mathrm{agg}}(z-1,t)}{F_{\mathrm{c}}\tau(z-1)}\right]. \tag{101}$$

Equation (101) can be further simplified by acknowledging that a series of compartments with constant mass and constant volume has the property

$$\frac{V_{\mathrm{real}}(z-1)}{V_{\mathrm{real}}(z)} = \frac{M_{\mathrm{real}}(z-1)}{M_{\mathrm{real}}(z)}, \tag{102}$$

and again applying the residence time definition to each compartment in (102) yields

$$\frac{V_{\mathrm{real}}(z-1)}{V_{\mathrm{real}}(z)} = \frac{\tau(z-1)}{\tau(z)}. \tag{103}$$

Substitution of (103) into (101) yields

$$R^{\mathrm{SWA}}_{\substack{\mathrm{inflow}\\ z\in\mathbb{L},\ z>1}}(z,t) = \left[\frac{V_{\mathrm{samp}}(z,t)}{V_{\mathrm{samp}}(z-1,t)}\right]\left[\frac{N_{\mathrm{agg}}(z-1,t)}{F_{\mathrm{c}}\tau(z)}\right]. \tag{104}$$

Now, if the inflow jump is to be coupled with the outflow jump process for any non-droplet zone ($z \neq 1$) then it is required that

$$R^{\mathrm{SWA}}_{\substack{\mathrm{inflow}\\ z\in\mathbb{L},\ z>1}}(z,t) = R^{\mathrm{SWA}}_{\substack{\mathrm{outflow}\\ z\in\mathbb{L},\ z>1}}(z,t) = \frac{N_{\mathrm{agg}}(z)}{\tau(z)}. \tag{105}$$

Finally, equating (104) and (105) yields an expression for the inflow weight scaling factor with the form

$$F_{\mathrm{c}}(z,t) = \left[\frac{V_{\mathrm{samp}}(z,t)}{V_{\mathrm{samp}}(z-1,t)}\right]\left[\frac{N_{\mathrm{agg}}(z-1,t)}{N_{\mathrm{agg}}(z,t)}\right]. \tag{106}$$

8. Appendix: layering rate equation

The layering source term in the primary particle PBE (2) has the form

$$\left.\frac{\mathrm{d}c_{\mathrm{pp}}}{\mathrm{d}t}\right|_{\mathrm{layer}} = -\int_{\mathbb{X}_{\mathrm{agg}}} r_{\mathrm{layer}}(z,t,x,c_{\mathrm{pp}})\lambda(z,t,\mathrm{d}x) \tag{107}$$

$$\approx -\frac{1}{V_{\mathrm{samp}}(z,t)}\sum_{i=1}^{N_{\mathrm{agg}(z,t)}} r_{\mathrm{layer}}(z,t,x_i,c_{\mathrm{pp}})w_i. \tag{108}$$

Hence, in number form

$$\left.\frac{\mathrm{d}N_{\mathrm{pp}}}{\mathrm{d}t}\right|_{\mathrm{layer}} \approx -\sum_{i=1}^{N_{\mathrm{agg}(z,t)}} r_{\mathrm{layer}}(z,t,x_i,c_{\mathrm{pp}})w_i, \tag{109}$$

and the change in the number of primaries over the global deferment step is then characterised as

$$N_{\mathrm{pp}}(z,t_{\mathrm{target}}) \leftarrow N_{\mathrm{pp}}(z,t) - \sum_{i=1}^{N_{\mathrm{agg}(z,t)}}\int_{t_{\mathrm{p}}}^{t_{\mathrm{target}}} r_{\mathrm{layer}}(z,t,x_i,c_{\mathrm{pp}})w_i\,\mathrm{d}t. \tag{110}$$

Re-arranging (28) gives

$$r_{\mathrm{layer}}(z,t,x,c_{\mathrm{pp}}) = \frac{1}{v_{\mathrm{pp}}}\left.\frac{\mathrm{d}s_{\mathrm{o}}(x)}{\mathrm{d}t}\right|_{\mathrm{layer}} \tag{111}$$

and since

$$\left.\frac{\mathrm{d}s_{\mathrm{o}}(x)}{\mathrm{d}t}\right|_{\mathrm{consol}} = 0, \tag{112}$$

then, by way of (37),

$$r_{\text{layer}}(z,t,x,c_{\text{pp}}) = \frac{1}{v_{\text{pp}}} \left.\frac{\mathrm{d}s_{\text{o}}(x)}{\mathrm{d}t}\right|_{\text{defer}}. \tag{113}$$

Substituting (113) into (110) and assuming that changes in N_{pp} over the deferment step are small yields

$$N_{\text{pp}}(z,t_{\text{target}}) \leftarrow N_{\text{pp}}(z,t) - \frac{1}{v_{\text{pp}}} \sum_{i=1}^{N_{\text{agg}(z,t)}} \left[s_{\text{o}}(x_i)_{t_{\text{target}}} - s_{\text{o}}(x_i)_{t_{\text{p}}}\right] w_i, \tag{114}$$

which completes the derivation.

The argument above can be applied in the context of local deferment steps by summing only over the sequence of particles which are involved in the local deferment step (and hence the subsequent jump process).

9. Appendix: derivation of primary particle transport rate

It is desired to show that the primary particle flow rate for a linear network of constant mass, constant volume compartments has the form

$$\left.\frac{\mathrm{d}N_{\text{pp}}(z)}{\mathrm{d}t}\right|_{\text{transport}} = \begin{cases} \dfrac{\dot{m}_{\text{feed}} V_{\text{samp}}(z,t)}{V_{\text{real}}(z)\rho_s v_{\text{pp}}} - \dfrac{N_{\text{pp}}(z,t)}{\tau(z)}, & \text{if } z = 1, \\ \dfrac{V_{\text{real}}(z-1)}{V_{\text{real}}(z)} \dfrac{V_{\text{samp}}(z)}{V_{\text{samp}}(z-1)} \dfrac{N_{\text{pp}}(z-1,t)}{\tau(z-1)} - \dfrac{N_{\text{pp}}(z,t)}{\tau(z)}, & \text{otherwise.} \end{cases} \tag{115}$$

Firstly, a component balance on the primary particles based on the transport processes (inflow and outflow) can be written with the form

$$\left.\frac{\mathrm{d}N_{\text{pp}}(z)}{\mathrm{d}t}\right|_{\text{transport}} = R_{\text{inflow,pp}}(z,t) - R_{\text{outflow,pp}}(z,t), \tag{116}$$

where $R_{\text{inflow,pp}}(z,t)$ and $R_{\text{outflow,pp}}(z,t)$ are the rates of primary particle inflow and outflow (number based) to/from the sample volume for compartment z, respectively. It is desired to define the forms of both terms of the RHS of (116) $\forall\, z \in \mathbb{L}$.

Firstly, consider the outflow term in (116). Using the mass-based definition of residence time the mass outflow rate of primary particles from the sample volume of compartment $z \; \forall \; z \in \mathbb{L}$ can be written as

$$\dot{m}^{\mathrm{SV}}_{\mathrm{pp,outflow}}(z) = \frac{M^{\mathrm{SV}}_{\mathrm{pp}}(z,t)}{\tau(z)}, \tag{117}$$

where $M^{\mathrm{SV}}_{\mathrm{pp}}(z,t)$ is the total mass hold-up of primary particles in the sample volume for compartment z.

Hence the rate of primary particle outflow from the sample volume of compartment z is

$$R_{\mathrm{outflow,pp}}(z,t) = \frac{\dot{m}^{\mathrm{SV}}_{\mathrm{pp,outflow}}(z)}{\rho_{\mathrm{s}} v_{\mathrm{pp}}} \tag{118}$$

$$= \frac{M^{\mathrm{SV}}_{\mathrm{pp}}(z,t)}{\rho_{\mathrm{s}} v_{\mathrm{pp}} \tau(z)}. \tag{119}$$

The total mass hold-up of primary particles can be written as

$$M^{\mathrm{SV}}_{\mathrm{pp}}(z,t) = N_{\mathrm{pp}}(z,t) \rho_{\mathrm{s}} v_{\mathrm{pp}}. \tag{120}$$

It follows from (119) and (120) that

$$R_{\mathrm{outflow,pp}}(z,t) = \frac{N_{\mathrm{pp}}(z,t)}{\tau(z)} \quad \forall z \in \mathbb{L}. \tag{121}$$

Moving on to the inflow term in the RHS or (116), firstly, consider the first reactor in the network i.e. $z = 1$. Since the mass feed to this compartment consists purely of primary particles, the mass feed rate to the physical first compartment is simply the operating mass feed rate i.e.

$$\dot{m}_{\mathrm{pp,inflow}}(1) = \dot{m}_{\mathrm{feed}}. \tag{122}$$

Thus, the mass feed rate of primary particles into the first compartment with sample volume $V_{\mathrm{samp}}(z,t)$ is

$$\dot{m}^{\mathrm{SV}}_{\mathrm{pp,inflow}}(1,t) = \dot{m}_{\mathrm{pp,inflow}}(1) \frac{V_{\mathrm{samp}}(1,t)}{V_{\mathrm{real}}(1)} \tag{123}$$

$$= \dot{m}_{\mathrm{feed}} \frac{V_{\mathrm{samp}}(1,t)}{V_{\mathrm{real}}(1)}. \tag{124}$$

The rate of primary particle inflow (number based) into the sample volume of the first compartment is then

$$R_{\text{inflow,pp}}(1,t) = \frac{\dot{m}^{\text{SV}}_{\text{pp,inflow}}(1,t)}{\rho_{\text{s}} v_{\text{pp}}} \tag{125}$$

$$= \frac{\dot{m}_{\text{feed}} V_{\text{samp}}(1,t)}{V_{\text{real}}(1)\rho_{\text{s}} v_{\text{pp}}}. \tag{126}$$

Together, (116), (121) and (126) prove (115) for the case $z = 1$.

In order to formulate an expression for $R_{\text{inflow,pp}}(z,t)\ \forall\ z \neq 1$, continuity (in terms of the primary particle phase) is enforced across the boundary between two compartments. This requires that the equality

$$R^{\text{real}}_{\text{inflow,pp}}(z,t) = R^{\text{real}}_{\text{outflow,pp}}(z-1,t)\ \ \forall\ z \neq 1 \tag{127}$$

be satisfied $\forall\ z \in \mathbb{L}, z > 1$, where $R^{\text{real}}_{\text{inflow,pp}}(z,t)$ and $R^{\text{real}}_{\text{inflow,pp}}(z,t)$ are the number flowrate of primary particles into and out of the physical compartment with indices z and $z-1$, respectively.

Suppose that the physical compartment z can be constructed from $n(z,t)$ identical sample volumes of size $V_{\text{samp}}(z,t)$. Applying the same logic to $z-1$, (127) may be expressed as

$$n(z,t)R_{\text{inflow,pp}}(z,t) = n(z-1,t)R_{\text{outflow,pp}}(z-1,t)\ \ \forall\ z \neq 1. \tag{128}$$

Since all sample volumes are identical, one may also write

$$n(z,t) = \frac{V_{\text{real}}(z)}{V_{\text{samp}}(z,t)}. \tag{129}$$

Substitution of (129) into (128) and re-arranging for $R_{\text{inflow,pp}}(z,t)$ yields

$$\underset{z\in\mathbb{L},\ z>1}{R_{\text{inflow,pp}}(z,t)} = \frac{V_{\text{real}}(z-1)}{V_{\text{real}}(z)} \frac{V_{\text{samp}}(z)}{V_{\text{samp}}(z-1)} R_{\text{outflow,pp}}(z-1,t). \tag{130}$$

Using the expression for $R_{\text{outflow,pp}}$ in (121) in (130) gives

$$\underset{z\in\mathbb{L},\ z>1}{R_{\text{inflow,pp}}(z,t)} = \frac{V_{\text{real}}(z-1)}{V_{\text{real}}(z)} \frac{V_{\text{samp}}(z)}{V_{\text{samp}}(z-1)} \frac{N_{\text{pp}}(z-1,t)}{\tau(z-1)}, \tag{131}$$

which, combined with (116) and (121), completes the derivation.

References

1. El Hagrasy A, Hennenkamp J, Burke M, Cartwright J, Litster J. Twin screw wet granulation: Influence of formulation parameters on granule properties and growth behavior. Powder Technology 2013;238:108 –15. doi:10.1016/j.powtec.2012.04.035.

2. Sayin R, El Hagrasy A, Litster J. Distributive mixing elements: Towards improved granule attributes from a twin screw granulation process. Chemical Engineering Science 2015;125:165 –75. doi:10.1016/j.ces.2014.06.040.

3. Lute SV, Dhenge RM, Hounslow MJ, Salman AD. Twin screw granulation: Understanding the mechanism of granule formation along the barrel length. Chemical Engineering Research and Design 2016;110:43 – 53. doi:10.1016/j.cherd.2016.03.008.

4. Meng W, Kotamarthy L, Panikar S, Sen M, Pradhan S, Marc M, Litster JD, Muzzio FJ, Ramachandran R. Statistical analysis and comparison of a continuous high shear granulator with a twin screw granulator: Effect of process parameters on critical granule attributes and granulation mechanisms. International Journal of Pharmaceutics 2016;513(1-2):357 – 75. doi:10.1016/j.ijpharm.2016.09.041.

5. Iveson SM, Litster JD, Hapgood K, Ennis BJ. Nucleation, growth and breakage phenomena in agitated wet granulation processes: a review. Powder Technology 2001;117(1-2):3 – 39. doi:10.1016/S0032-5910(01)00313-8.

6. Vercruysse J, Peeters E, Fonteyne M, Cappuyns P, Delaet U, Assche IV, Beer TD, Remon J, Vervaet C. Use of a continuous twin screw granulation and drying system during formulation development and process optimization. European Journal of Pharmaceutics and Biopharmaceutics 2015;89:239 –47. doi:10.1016/j.ejpb.2014.12.017.

7. Shah U. Use of a modified twin-screw extruder to develop a high-strength tablet dosage form. Pharmaceutical technology 2005;29(6):52–66.

8. Vercruysse J, Burggraeve A, Fonteyne M, Cappuyns P, Delaet U, Assche IV, Beer TD, Remon J, Vervaet C. Impact of screw configuration on the particle size distribution of granules produced by twin screw granulation. International Journal of Pharmaceutics 2015;479(1):171 –80. doi:10.1016/j.ijpharm.2014.12.071.

9. Pradhan SU, Sen M, Li J, Litster JD, Wassgren CR. Granule breakage in twin screw granulation: Effect of material properties and screw element geometry. Powder Technology 2017;315(Supplement C):290 –9. doi:10.1016/j.powtec.2017.04.011.

10. Kumar A, Vercruysse J, Bellandi G, Gernaey KV, Vervaet C, Remon JP, Beer TD, Nopens I. Experimental investigation of granule size and shape dynamics in twin-screw granulation. International Journal of Pharmaceutics 2014;475(1-2):485 –95. doi:10.1016/j.ijpharm.2014.09.020.

11. El Hagrasy AS, Litster JD. Granulation rate processes in the kneading elements of a twin screw granulator. AIChE Journal 2013;59(11):4100–15. doi:10.1002/aic.14180.

12. Ramkrishna D. Population Balances: Theory and Applications to Particulate Systems in Engineering. Elsevier Science; 2000.

13. Barrasso D, Walia S, Ramachandran R. Multi-component population balance modeling of continuous granulation processes: A parametric study and comparison with experimental trends. Powder Technology 2013;241:85 – 97.

14. Barrasso D, Eppinger T, Pereira FE, Aglave R, Debus K, Bermingham SK, Ramachandran R. A multi-scale, mechanistic model of a wet granulation process using a novel bi-directional PBM-DEM coupling algo-

rithm. Chemical Engineering Science 2015;123:500 –13. doi:10.1016/j.ces.2014.11.011.

15. Barrasso D, El Hagrasy A, Litster JD, Ramachandran R. Multi-dimensional population balance model development and validation for a twin screw granulation process. Powder Technology 2015;270, Part B:612 –21. doi:10.1016/j.powtec.2014.06.035.

16. Kumar A, Gernaey KV, Beer TD, Nopens I. Model-based analysis of high shear wet granulation from batch to continuous processes in pharmaceutical production - A critical review. Eur J Pharm Biopharm 2013;85(3, Part B):814 –32.

17. Kumar A, Vercruysse J, Mortier ST, Vervaet C, Remon JP, Gernaey KV, Beer TD, Nopens I. Model-based analysis of a twin-screw wet granulation system for continuous solid dosage manufacturing. Computers & Chemical Engineering 2016;89:62 – 70. doi:10.1016/j.compchemeng.2016.03.007.

18. Kumar S, Ramkrishna D. On the solution of population balance equations by discretization-I. a fixed pivot technique. Chemical Engineering Science 1996;51(8):1311 –32. doi:10.1016/0009-2509(96)88489-2.

19. Kumar S, Ramkrishna D. On the solution of population balance equations by discretization-II. a moving pivot technique. Chemical Engineering Science 1996;51(8):1333 –42. doi:10.1016/0009-2509(95)00355-X.

20. Kumar S, Ramkrishna D. On the solution of population balance equations by discretization-III. nucleation, growth and aggregation of particles. Chemical Engineering Science 1997;52(24):4659 –79. doi:10.1016/S0009-2509(97)00307-2.

21. Rjasanow S, Wagner W. A stochastic weighted particle method for the

Boltzmann equation. Journal of Computational Physics 1996;124(2):243 – 53. doi:10.1006/jcph.1996.0057.

22. Eibeck A, Wagner W. Stochastic particle approximations for Smoluchoski's coagulation equation. The Annals of Applied Probability 2001;11(4):1137–65.

23. Patterson RIA, Wagner W, Kraft M. Stochastic weighted particle methods for population balance equations. Journal of Computational Physics 2011;230(19):7456 –72. doi:10.1016/j.jcp.2011.06.011.

24. Patterson RIA, Wagner W. A stochastic weighted particle method for coagulation–advection problems. SIAM Journal on Scientific Computing 2012;34(3):B290–311. doi:10.1137/110843319. arXiv:10.1137/110843319.

25. Zhao H, Zheng C, Xu M. Multi-Monte Carlo approach for general dynamic equation considering simultaneous particle coagulation and breakage. Powder Technology 2005;154(2-3):164 –78. doi:10.1016/j.powtec.2005.04.042.

26. Zhao H, Zheng C. A new event-driven constant-volume method for solution of the time evolution of particle size distribution. Journal of Computational Physics 2009;228(5):1412 –28. doi:10.1016/j.jcp.2008.10.033.

27. Zhao H, Kruis FE, Zheng C. A differentially weighted Monte Carlo method for two-component coagulation. Journal of Computational Physics 2010;229(19):6931 –45. doi:10.1016/j.jcp.2010.05.031.

28. Zhao H, Zheng C. A population balance-Monte Carlo method for particle coagulation in spatially inhomogeneous systems. Computers & Fluids 2013;71:196 – 207. doi:10.1016/j.compfluid.2012.09.025.

29. Gantt JA, Gatzke EP. A stochastic technique for multidimensional granulation modeling. AIChE Journal 2006;52(9):3067–77. doi:10.1002/aic.10911.

30. Braumann A, Goodson MJ, Kraft M, Mort PR. Modelling and validation of granulation with heterogeneous binder dispersion and chemical reaction. Chemical Engineering Science 2007;62(17):4717 –28. doi:10.1016/j.ces.2007.05.028.

31. Braumann A, Man PLW, Kraft M. Statistical approximation of the inverse problem in multivariate population balance modeling. Journal of Industrial and Engineering Chemistry 2010;49(1):428–38. doi:10.1021/ie901230u.

32. Braumann A, Kraft M, Mort PR. Parameter estimation in a multidimensional granulation model. Powder Technology 2010;197(3):196 – 210. doi:10.1016/j.powtec.2009.09.014.

33. Braumann A, Kraft M. Incorporating experimental uncertainties into multivariate granulation modelling. Chemical Engineering Science 2010;65(3):1088 –100. doi:10.1016/j.ces.2009.09.063.

34. Braumann A, Man PLW, Kraft M. The inverse problem in granulation modeling-two different statistical approaches. AIChE Journal 2011;57(11):3105–21. doi:10.1002/aic.12526.

35. Braumann A, Kraft M, Wagner W. Numerical study of a stochastic particle algorithm solving a multidimensional population balance model for high shear granulation. Journal of Computational Physics 2010;229(20):7672 – 91. doi:10.1016/j.jcp.2010.06.021.

36. Lee KF, Mosbach S, Kraft M, Wagner W. A multicompartment population balance model for high shear granulation. Computers & Chemical Engineering 2015;75:1 – 13. doi:10.1016/j.compchemeng.2015.01.009.

37. Lee KF, Patterson RIA, Wagner W, Kraft M. Stochastic weighted particle methods for population balance equations with coagulation, fragmentation and spatial inhomogeneity. Journal of Computational Physics 2015;303:1 – 18. doi:10.1016/j.jcp.2015.09.031.

805 38. Menz WJ, Akroyd J, Kraft M. Stochastic solution of population balance equations for reactor networks. Journal of Computational Physics 2014;256:615–29.

39. Boje A, Akroyd J, Sutcliffe S, Edwards J, Kraft M. Detailed population balance modelling of TiO2 synthesis in an industrial reactor. 810 Chemical Engineering Science 2017;164:219 –31. doi:10.1016/j.ces.2017.02.019.

40. Mosbach S, Su H, Kraft M, Bhave A, Mauss F, Wang Z, Wang JX. Dual injection homogeneous charge compression ignition engine simulation using a stochastic reactor model. 815 International Journal of Engine Research 2007;8(1):41–50. doi:10.1243/14680874JER01806. arXiv:10.1243/14680874JER01806.

41. Cao L, Su H, Mosbach S, Kraft M, Bhave A, Kook S, Bae C. Studying the influence of direct injection on PCCI combustion and emissions at engine idle condition using two dimensional CFD and stochastic reactor model. 820 2008. doi:10.4271/2008-01-0021; sAE Technical Paper No. 2008-01-0021. doi:10.4271/2008-01-0021.

42. McGuire AD, Mosbach S, Lee KF, Reynolds G, Kraft M. A high-dimensional, stochastic model for twin-screw granulation–part 1: Model description. Chem Eng Sci 2018;188:221–37. doi:10.1016/j.ces.2018.04.076. 825

43. McGuire AD, Mosbach S, Lee KF, Reynolds G, Kraft M. A high-dimensional, stochastic model for twin-screw granulation part 2: Numerical methodology. Chem Eng Sci 2018;188:18–33. doi:10.1016/j.ces.2018.04.077.

44. Patterson RIA, Singh J, Balthasar M, Kraft M, Norris J. The linear process deferment algorithm: A new technique for solving population balance equations. SIAM Journal on Scientific Computing 2006;28(1):303–20.

45. Tan H, Goldschmidt M, Boerefijn R, Hounslow M, Salman A, Kuipers J. Building population balance model for fluidized bed melt granulation: lessons from kinetic theory of granular flow. Powder Technology 2004;142(2-3):103 –9.

46. Cundall PA, Strack OD. A discrete numerical model for granular assemblies. Geotechnique 1979;29(1):47–65.

47. Lee KF, Dosta M, McGuire AD, Mosbach S, Wagner W, Heinrich S, Kraft M. Development of a multi-compartment population balance model for high-shear wet granulation with discrete element method. Computers & Chemical Engineering 2017;99:171 –84. doi:10.1016/j.compchemeng.2017.01.022.

48. Barrasso D, Ramachandran R. Qualitative assessment of a multi-scale, compartmental PBM-DEM model of a continuous twin-screw wet granulation process. Journal of Pharmaceutical Innovation 2016;11(3):231–49. doi:10.1007/s12247-015-9240-7.

49. Kumar A, Vercruysse J, Toiviainen M, Panouillot PE, Juuti M, Vanhoorne V, Vervaet C, Remon JP, Gernaey KV, Beer TD, Nopens I. Mixing and transport during pharmaceutical twin-screw wet granulation: Experimental analysis via chemical imaging. European Journal of Pharmaceutics and Biopharmaceutics 2014;87(2):279 –89. doi:10.1016/j.ejpb.2014.04.004.

50. Kumar A, Vercruysse J, Vanhoorne V, Toiviainen M, Panouillot PE, Juuti M, Vervaet C, Remon JP, Gernaey KV, Beer TD, Nopens I. Conceptual framework for model-based analysis of residence time distribution in twin-screw granulation. European Journal of Pharmaceutical Sciences 2015;71:25 – 34.

51. Barrasso D, Eppinger T, Pereira FE, Aglave R, Debus K, Bermingham SK, Ramachandran R. A multi-scale, mechanistic model of a wet granulation process using a novel bi-directional PBM–DEM coupling algorithm. Chemical Engineering Science 2015;123:500–13.

52. Barrasso D, Tamrakar A, Ramachandran R. Model order reduction of a multi-scale PBM-DEM description of a wet granulation process via ANN. Procedia Engineering 2015;102(Supplement C):1295 –304. doi:doi.org/10.1016/j.proeng.2015.01.260.

53. Seem TC, Rowson NA, Gabbott I, de Matas M, Reynolds GK, Ingram A. Asymmetric distribution in twin screw granulation. European Journal of Pharmaceutics and Biopharmaceutics 2016;106:50 –8. doi:10.1016/j.ejpb.2016.01.013.

54. Lee KT, Ingram A, Rowson NA. Twin screw wet granulation: The study of a continuous twin screw granulator using positron emission particle tracking (PEPT) technique. European Journal of Pharmaceutics and Biopharmaceutics 2012;81(3):666 –73. doi:10.1016/j.ejpb.2012.04.011.

55. Gorringe L, Kee G, Saleh M, Fa N, Elkes R. Use of the channel fill level in defining a design space for twin screw wet granulation. International Journal of Pharmaceutics 2017;519(1):165 –77. doi:10.1016/j.ijpharm.2017.01.029.

56. Saleh MF, Dhenge RM, Cartwright JJ, Hounslow MJ, Salman AD. Twin screw wet granulation: Effect of process and formulation variables on powder caking during production. International Journal of Pharmaceutics 2015;496(2):571 –82. doi:10.1016/j.ijpharm.2015.10.069.

57. Eitzlmayr A, Koscher G, Reynolds G, Huang Z, Booth J, Shering P, Khinast J. Mechanistic modeling of modular co-rotating twin-screw extruders. International Journal of Pharmaceutics 2014;474(1-2):157 –76. doi:10.1016/j.ijpharm.2014.08.005.

58. Meier R, Moll KP, Krumme M, Kleinebudde P. Impact of fill-level in twin-screw granulation on critical quality attributes of granules and tablets. European Journal of Pharmaceutics and Biopharmaceutics 2017;115(Supplement C):102 –12. doi:10.1016/j.ejpb.2017.02.010.

59. Rjasanow S, Wagner W. Simulation of rare events by the stochastic weighted particle method for the Boltzmann equation. Mathematical and Computer Modelling 2001;33(8):907 –26. doi:10.1016/S0895-7177(00)00289-2.

60. Menz WJ, Patterson RIA, Wagner W, Kraft M. Application of stochastic weighted algorithms to a multidimensional silica particle model. Journal of Computational Physics 2013;248(0):221–34. doi:10.1016/j.jcp.2013.04.010.

61. Gillespie DT. An exact method for numerically simulating the stochastic coalescence process in a cloud. Journal of the Atmospheric Sciences 1975;32(10):1977–89.

62. Celnik M, Patterson RIA, Kraft M, Wagner W. Coupling a stochastic soot population balance to gas-phase chemistry using operator splitting. Combustion and Flame 2007;148(3):158 –76. doi:10.1016/j.combustflame.2006.10.007.

63. Patterson RIA. Convergence of stochastic particle systems undergoing advection and coagulation. Stochastic Analysis and Applications 2013;31(5):800–29. doi:10.1080/07362994.2013.817245.

64. Eibeck A, Wagner W. Approximative solution of the coagulation-fragmentation equation by stochastic particle systems. Stochastic Analysis and Applications 2000;18(6):921–48. doi:10.1080/07362990008809704.

65. Goodson M, Kraft M. Simulation of coalescence and breakage: an assessment of two stochastic methods suitable for simulating liquid-liquid extrac-

tion. Chemical Engineering Science 2004;59(18):3865 –81. doi:10.1016/j.ces.2004.05.029.

66. Hao X, Zhao H, Xu Z, Zheng C. Population balance-Monte Carlo simulation for gas-to-particle synthesis of nanoparticles. Aerosol science and technology 2013;47(10):1125–33.

67. McGuire AD, Lee KF, Dosta M, Mosbach S, Rosenboom JG, Heinrich S, Kraft M. Compartmental residence time estimation in batch granulators using a colourimetric image analysis algorithm and discrete element modelling. Advanced Powder Technology 2017;28(9):2239 –55. doi:10.1016/j.apt.2017.06.005.

68. Zadow JG. Lactose: Properties and uses. Journal of Dairy Science 1984;67(11):2654–79. doi:10.3168/jds.S0022-0302(84)81625-2.

69. Bratley P, Fox BL. Algorithm 659: Implementing Sobol's quasirandom sequence generator. ACM Transactions on Mathematical Software 1988;14(1):88–100. doi:10.1145/42288.214372.

70. Hooke R, Jeeves TA. "Direct search" solution of numerical and statistical problems. Journal of the ACM 1961;8(2):212–29. doi:10.1145/321062.321069.

71. MoDS . (Model Development Suite). Cambridge, United Kingdom: CMCL Innovations; 2015. https://cmclinnovations.com/products/mods/.

72. Seem TC, Rowson NA, Ingram A, Huang Z, Yu S, de Matas M, Gabbott I, Reynolds GK. Twin screw granulation - a literature review. Powder Technology 2015;276:89 – 102. doi:10.1016/j.powtec.2015.01.075.

73. Dhenge RM, Cartwright JJ, Hounslow MJ, Salman AD. Twin screw wet granulation: Effects of properties of granulation liquid. Powder Technology 2012;229:126 –36. doi:10.1016/j.powtec.2012.06.019.

74. Vercruysse J, Díaz DC, Peeters E, Fonteyne M, Delaet U, Assche IV, Beer TD, Remon J, Vervaet C. Continuous twin screw granulation: Influence of process variables on granule and tablet quality. European Journal of Pharmaceutics and Biopharmaceutics 2012;82(1):205–11. doi:10.1016/j.ejpb.2012.05.010.